Geochimica et Cosmochimica Acta 382 (2024) 128–141

Contents lists available at ScienceDirect

Geochimica et Cosmochimica Acta

journal homepage: www.elsevier.com/locate/gca

Stability and transformation of jarosite and Al-substituted jarosite in an acid sulfate paddy soil under laboratory and field conditions

Andrew R.C. Grigg [a,*], Worachart Wisawapipat [b], Kurt Barmettler [a], Katrin Schulz [a], Luiza Notini [a], Laurel K. ThomasArrigo [a,c], Ruben Kretzschmar [a]

[a] Soil Chemistry Group, Institute of Biogeochemistry and Pollutant Dynamics, Department of Environmental Systems Science, ETH Zurich, Universitätstrasse 16, CHN, 8092 Zurich, Switzerland
[b] Department of Soil Science, Faculty of Agriculture, Kasetsart University, Bangkok 10900, Thailand
[c] Environmental Chemistry Group, Institute of Chemistry, University of Neuchâtel, Avenue de Bellevaux 51, 2000 Neuchâtel, Switzerland

ARTICLE INFO

Associate editor: Elizabeth Herndon

Keywords:
Iron minerals
Mössbauer spectroscopy
Redox
Rice paddy
Soil incubation

ABSTRACT

Jarosite, a prominent mineral in oxidised acid sulfate soil, is known to sorb and incorporate a variety of elements, including Al. However, to understand the role that jarosite plays in regulating element cycles, it is crucial to understand the stability and transformation pathways of jarosite in an acid sulfate soil under dynamic biogeochemical conditions. In this study, we observed the transformation of unsubstituted jarosite and Al-substituted jarosite, collectively referred to as 'jarosite', in an acid-sulfate rice paddy topsoil and subsoil from Thailand. Jarosite was incubated in flooded paddy topsoils and subsoils for up to sixteen weeks, both in laboratory mesocosms and in the field, using bags made of polyethylene terephthalate mesh. One set of mesh bags contained jarosite that was not mixed with any other minerals, and referred to as 'pure mineral' incubations. Mineral transformations occurred under the influence of the soil porewater only and were primarily followed by X-ray diffraction analysis. A parallel set of mesh bags contained soil with ^{57}Fe-labelled jarosite enrichment (Fe enriched in soil by a factor of 1.3 but ^{57}Fe enrichment factor of 12.5–13.6), which allowed jarosite transformation to occur in close association with the soil matrix. Mineral transformations in ^{57}Fe-jarosite-enriched soil were followed using ^{57}Fe Mössbauer spectroscopy. In laboratory mesocosms and in the field, jarosite transformed most quickly in topsoil, whereas jarosite underwent limited transformation in subsoils, especially in laboratory mesocosms where Fe reduction was slow. The chemical environment around the jarosite affected the outcome of the transformation processes. Crystalline Fe oxyhydroxides, such as goethite, dominated the products in mesh bags where jarosite was not mixed with soil, whereas short-range-ordered or non-mineral Fe phases, such as Fe(II) sorbed to mineral surfaces or complexed with organic ligands, were dominant transformation products of jarosite when mixed in soil. Furthermore, Al substitution in jarosite caused contrasting effects in mesh bags containing pure minerals or mineral-enriched soil. Aluminium substitution slowed the transformation of jarosite in pure mineral mesh bags, but Al-substituted and unsubstituted jarosite showed similar transformation rates and pathways when incubated as a mixture with soil. The contrasting rate of transformation in topsoil and subsoil, the contrasting products of transformation in pure mineral mesh bags and ^{57}Fe-jarosite-enriched soil, and the contrasting effect of Al substitution in pure mesh bags or jarosite-enriched soil, all demonstrate that the rate and products of jarosite transformation are defined by a balance between competitive transformation pathways that affect the transforming minerals.

1. Introduction

Jarosite is a potassium-iron hydroxysulfate mineral commonly found in acidic environments, such as acid sulfate soils (ASS) and acid mine drainage environments. As a member of the alunite supergroup of minerals, jarosite has the general formula $AB_3(TO_4)_2(OH)_6$ with the A site being dominated by K, the B site containing mostly Fe(III), and the T site being occupied by S (Menchetti and Sabelli, 1976). Jarosite only forms under oxic (Eh > +400 mV), acidic (pH ~2–4) conditions in the presence of Fe(III) and SO_4 (Van Breemen, 1982). Most prominently,

* Corresponding author.
E-mail address: andrew.grigg@usys.ethz.ch (A.R.C. Grigg).

https://doi.org/10.1016/j.gca.2024.07.026
Received 28 March 2024; Accepted 22 July 2024
Available online 26 July 2024

jarosite occurs in ASS as pale yellow mottles (cm-scale regions within the soil that are highly enriched in jarosite) that form soil coatings within voids following the oxidation of pyrite (Poch et al., 2009; Van Breemen, 1982). Jarosite mottles are indicative of acidic aqueous environments, and are a diagnostic feature of active acid sulfate horizons in some soil taxonomy systems, including the thionic horizons of the World Reference Base for Soil Resources (WRB) (IUSS Working Group WRB, 2015, 2022), sulfuric horizons in the United States Department of Agriculture (USDA) classification system (Soil Survey Staff, 2015), and various soil series of the Central Plain region within the Thai soil classification system (Land Development Department, 2004).

Jarosite plays an important role as a scavenger of trace and major elements in ASS, as well as in other natural and engineered systems. Potentially toxic elements have been shown to associate with jarosite, either structurally incorporated as oxyanions, such as AsO_4^{3-} or CrO_4^{2-} (Karimian et al., 2018; Ryu and Kim, 2022), structurally incorporated as cations, such as Na^+, Sr^{2+} or Al^{3+} (Grigg et al., 2024b; Stoffregen et al., 2000; Welch et al., 2007), or associated with jarosite surfaces by sorption such as As or Sb (Karimian et al., 2023). In some situations, jarosite formation is induced in industrial processes or for remediation of contaminated soil to immobilise impurities or pollutants, such as Pb, S and alkali metals (Dutrizac and Jambor, 2000; Karna et al., 2021). In addition to its load of trace elements, jarosite may release acidity by the hydrolysis of Fe(III) upon dissolution, which may present an environmental hazard if released to the soil porewater (Vithana et al., 2013). Since dissolution of jarosite can mobilise toxic elements (Welch et al., 2007), the mobility and distribution of these elements in the soil profile is dependent on the formation, stability and transformation pathways of jarosite (Sukitprapanon et al., 2020).

The stability of jarosite in ASS remains a matter of debate (Sukitprapanon et al., 2020). Jarosite has a narrow thermodynamic stability field in acid sulfate systems (Alpers et al., 1989; Van Breemen and Harmsen, 1975), but it has been observed in oxidised ASS decades after its initial formation (Trueman et al., 2020; Van Breemen and Harmsen, 1975). In well-mixed mineral suspensions, synthetic jarosite dissolves slowly at low pH, with a minimum dissolution rate at pH 3.5, but dissolution rates increase at higher pH, up to at least pH 10.9 (Elwood Madden et al., 2012). Under anoxic conditions, Fe(II)-catalysed transformation is not observed in batch experimental systems at pH < 4.0 (Karimian et al., 2018), but Fe(II)-catalysis has been shown to be a major driver of jarosite transformation to goethite, lepidocrocite, magnetite and green rust between pH 5.5 and 7.0 (Grigg et al., 2024a; Karimian et al., 2017, 2018). In addition, sulfidation of jarosite occurs throughout a wide pH range, from as low as pH 4.0 to at least pH 8.0 (Johnston et al., 2012). Experiments that employ well-mixed mineral suspensions have also been used to demonstrate that jarosite dissolution is accelerated in the presence of pure cultures or consortia of sulfate-reducing bacteria (SRB) at circumneutral pH (Gao et al., 2019; Ivarson and Hallberg, 1976) and Fe-reducing bacteria at low pH (pH 2.0 & 2.8; Bridge and Johnson, 2000), circumneutral (Jones et al., 2006), and high pH values (pH up to 8.0; Ouyang et al., 2014). Factors which affect the mineral structure, such as the substitution, incorporation, or sorption of organic and inorganic compounds, further influence the rate and pathway of jarosite dissolution and transformation. For example, Al substitution for Fe (Grigg et al., 2024a), oxyanion substitution for SO_4 (Ryu and Kim, 2022) and sorption of Si and natural organic matter (Jones et al., 2009) slow the rate of jarosite transformation, and change the balance of lepidocrocite, ferrihydrite and goethite in the products.

Although experiments in well-mixed mineral suspensions have highlighted key aspects of jarosite reactivity, these systems do not replicate the complexity of porewater composition, pore-scale advective or diffusive processes, direct interactions with organic and inorganic soil components, and the influence of native soil biological communities. Therefore, mixed suspension studies are complemented by observations of in situ jarosite dynamics in ASS based on interpretation of the distribution (Sukitprapanon et al., 2016; Van Breemen and Harmsen, 1975) and morphology (Keene et al., 2010) of jarosite that is present in ASS profiles. These field observations show that the stability of jarosite in acid sulfate rice paddy soil depends on differences in the geochemical conditions in each horizon and temporal differences in geochemical conditions induced by flooding-draining cycles (Sukitprapanon et al., 2016; Van Breemen and Harmsen, 1975). However, the rate and pathways of the transformations could not be assessed directly in the field studies.

To bridge the gap between studies with well-mixed mineral suspensions and in situ observations, there is increasing interest in experiment methods that allow investigations of mineral transformation under biogeochemical conditions that occur in soil. For example, a study of jarosite in the environment, in which perforated plastic tubes were used to incubate synthetic jarosite in acidic surface water and neutral anoxic sediments in a catchment that drains ASS, showed that jarosite partially transformed to goethite in one year (Vithana et al., 2015). The result stood in contrast to the transformation of synthetic jarosite in well-mixed mineral suspensions using environmentally relevant pH (between 4 and 7) and ratios of Fe(II) to Fe(III), which typically transform to goethite within hours or days (Grigg et al., 2024a; Jones et al., 2009; Karimian et al., 2017, 2018). Novel methods that have been used to follow the transformations of synthetic Fe (oxyhydr)oxides during incubation in soils, such as mesh bags (Grigg et al., 2022; Nielsen et al., 2014; Vogelsang et al., 2016), diffusive gels (Kraal et al., 2020), and ^{57}Fe isotopic labelling (Notini et al., 2023; Schulz et al., 2023), offer new insights into the effect of close contact with soil on mineral transformation processes. These studies have shown that transformation processes take months or years in soil (Grigg et al., 2022; Kraal et al., 2020; Nielsen et al., 2014; Notini et al., 2023; Schulz et al., 2023; Vogelsang et al., 2016), which is longer than the transformation typically observed in well-mixed mineral suspensions with similar Fe(II) concentrations and pH (Boland et al., 2013; Boland et al., 2014; Pedersen et al., 2005; Tronc et al., 1992; Yang et al., 2010; Yee et al., 2006).

This study was designed to explore reasons for the persistence of jarosite in ASS profiles that are subject to regular flooding-drainage cycles, using incubation techniques that support investigations of the effects of the soil matrix on the rate and pathway of Fe mineral transformations. The aims were, firstly, to assess how the biogeochemical conditions in porewater from typical ASS topsoils and subsoils affect the rate and pathway of synthetic jarosite transformation, secondly, to investigate the effect of direct proximity to the soil matrix on the rate and pathway of jarosite transformation, and thirdly, to assess what effect Al-for-Fe substitution of the synthetic jarosite has on the rate and products of jarosite transformation when reacted with soil porewater and within the complex matrix. The rates and pathways of synthetic jarosite and Al-substituted jarosite transformation were measured during lab and field incubation of two horizons of an acid sulfate rice paddy soil from Chachoengsao province, Thailand. The results extend the current understanding of jarosite reactivity that is based on mixed-suspension systems (Grigg et al., 2024a) to laboratory-scale and field-scale experiments involving incubation in soil, to show how the interaction of competing transformation pathways explains the Fe mineral composition of ASS at different stages of its evolution due to dependence of the transformation pathways on the soil environment.

2. Methods

2.1. Overview and soil preparation

The study was designed in two parts whereby identical synthetic jarosite samples were incubated in a laboratory mesocosm experiment using two soils collected from a rice paddy in Thailand, and directly in the field in soils from the same profile horizons. The laboratory mesocosm experiment was carried out to maximise control, in terms of the homogeneity of the incubation soil and the frequency of the porewater sampling. The field experiment was conducted to confirm that the

results of the laboratory mesocosm were relevant under field conditions. The soil used in this study was a Hydragric Vertic Anthrosol in the WRB classification system (IUSS Working Group WRB, 2015) belonging to the Rangsit series in the Thai soil classification system (Land Development Department, 2004), found at the Chachoengsao Rice Research Centre in Chachoengsao province, Thailand (Grigg et al., 2024b). For the initial investigation, a soil profile was excavated to 180 cm depth (Fig. S1) during the dry season in February 2020 from which samples were collected for laboratory mesocosm experiments and to prepare soil-mineral mixtures (Section 2.2). Topsoil samples were collected from the upper 30 cm to represent the most biogeochemically active layer, above the plough pan. Subsoils were collected from 50 to 80 cm depth, which lies immediately below the plough pan, but above the sulfide-bearing layer, in the upper part of the jarosite-bearing layer. Soils were sent to Switzerland, dried at 30 °C, and sieved to 2 mm. Soil geochemical and textural composition are listed in Section S1.

2.2. Mineral sample preparation

The mineral samples were synthetic unsubstituted jarosite (henceforth unsubstituted jarosite) or synthetic Al-substituted jarosite (henceforth Al-jarosite), collectively called 'jarosite'. Unsubstituted jarosite and Al-jarosite were both synthesised with natural-isotope-abundance Fe and ^{57}Fe-enrichment (henceforth called ^{NA}Fe-jarosite and ^{57}Fe-jarosite, respectively), according to a hydrothermal method previously described (Grigg et al., 2024b). Briefly, ^{NA}Fe(0) powder (10 μm metal powder, EMSURE analysis grade, Merck) or ^{57}Fe-enriched Fe(0) powder (96.14 % ^{57}Fe, Isoflex, USA) was dissolved in 2 M sulfuric acid (95–97 % reagent grade, Sigma Aldrich), filtered with a 0.22 μm nylon syringe filter and oxidised with excess H_2O_2 (35 %, Merck). To synthesise Al-jarosite, 0.3 M $AlK(SO_4)_2{\cdot}12H_2O$ (supplied as salt, Normapur reagent grade, VWR) solution was mixed with the 0.9 M Fe(III) solution to produce a final Al:Fe ratio of 3:7. The Fe or Fe-Al solutions were adjusted to pH 2.5 with KOH ('Pellets extra pure', Merck), heated to 140 °C for 5 h in a sealed Teflon vessel, then the precipitated solids were decanted, rinsed, dried at 60 °C for 24 h and stored in amber glass in a desiccator until use. To ensure chemical and structural purity, synthesised jarosite samples were characterised by powder X-ray diffraction (XRD) and samples were dissolved in 4 M HCl (Normatom, VWR) for elemental composition analysis using inductively coupled plasma with optical emission spectroscopy (ICP-OES, 5100, Agilent Technologies) for Fe, S and Al or atomic absorbance spectroscopy (AAS, 240FS spectrometer, Agilent Technologies) at 766.5 nm with sample atomisation in an air-acetylene flame for K. The Al-^{NA}Fe-jarosite and Al-^{57}Fe-jarosite had Al/(Fe + Al) of 0.10 and 0.08, respectively (Table S2). Further mineral properties are reported in Section S2.

The ^{57}Fe-jarosite-enriched soils were mixtures of 700 mg of topsoil or subsoil, with sufficient ^{57}Fe-jarosite to ensure that the ^{57}Fe signal measured by Mössbauer spectroscopy was dominated by ^{57}Fe that was added in synthetic mineral additions to the soil (Notini et al., 2023). Topsoils and subsoils naturally contain approximately 1.9 % (w/w) and 3.6 % (w/w) ^{NA}Fe, respectively, and ^{57}Fe comprises 2.119 % of ^{NA}Fe (Taylor et al., 1992). Therefore, topsoil was spiked with 13 mg and subsoils with 25 mg ^{57}Fe-jarosite, which corresponded to a theoretical total Fe enrichment of 29 % in unsubstituted-jarosite-enriched soil and 26 % in Al-jarosite-enriched soil. According to these calculations, between 92 % and 93 % of the ^{57}Fe in the enriched soils was added as ^{57}Fe-jarosite. The measured ^{57}Fe enrichment in samples, as prepared for incubation, is reported in Table S5.

Mineral samples in both field and mesocosm experiments were deployed in mesh bags made of polyethylene terephthalate (PETE) mesh fabric with pore size of 51 μm (Sefar, Switzerland) with approximate internal dimensions of 30 × 10 × 2 mm when filled. The mesh fabric was triple layered to minimise mineral loss and closed with a heat seal. Each mesh bag contained either 100 mg of pure (meaning not mixed with soil) ^{NA}Fe-jarosite, 713 mg of ^{57}Fe-jarosite-enriched topsoil or 725 mg of ^{57}Fe-jarosite-enriched subsoil. Mesh bags were inserted into soils vertically using 3D-printed sample holders, which were fixed to threaded nylon rods for mesocosms and field topsoils, or acrylic rods via a Teflon-tape-coated screw for field subsoils. Detail about the sample holder design is described in Section S3 and design files are available for download in the Supplementary dataset.

2.3. Laboratory mesocosm incubation experiment

Laboratory mesocosms were constructed from six plastic containers with internal dimensions of 37.6 × 26.0 × 28.3 cm similar to those used in Schulz et al. (2023). Each mesocosm contained 10 kg of oven-dry (30 °C) topsoil or subsoil, which was saturated with 6 L of ultra-pure water (UPW, MilliQ, >18.2 MΩ cm), such that the soils were fully submerged. Air pockets were removed by agitating the soils before samples or samplers were deployed. The wet soil had a depth of approximately 15 cm in the containers. The mesocosms were stored at 30 °C throughout the incubation period and covered in plastic film to limit evaporation. Evaporation was compensated by 300 mL additions of UPW after sampling at six and twelve weeks.

Triplicate sets of the mineral samples described in Section 2.2 were deployed in mesocosms to a depth of 10 cm, measured to the centroid of the mesh bag. Samples were arranged to ensure that all replicate samples were incubated in different mesocosms (i.e., each mesocosm is considered a complete replicate) and not located in the equivalent location within replicate mesocosms (Fig. S3). Samples were removed from the soil after four, eight or sixteen weeks and immediately closed in a nitrogen-flushed tube for transport to the glovebox (MBRAUN; N_2 atmosphere). In the glovebox, the sample holders were cut open and the mesh bags were removed. The mesh bags were dried over at least 24 h in the glovebox atmosphere, before the contents were removed from the mesh bags and gently crushed with mortar and pestle. All samples were stored in the dark in a glovebox until analysed.

Porewater was extracted from mesocosms at selected time intervals throughout the incubation period by suction through Rhizon samplers (Rhizosphere Research, NL; model 'flex', 5 cm-long porous filter with 0.6 μm cut-off) which were pre-positioned in the centre of each mesocosm (Fig. S3). Porewater for dissolved organic carbon (DOC) analysis was immediately filtered through a 0.45 μm nylon filter and then acidified to pH 3–4 with concentrated HCl. Porewater for elemental analysis using ICP-OES was filtered through a 0.22 μm nylon filter and then acidified in 1 % HCl. For full porewater sampling details see Section S5.2. Porewater analysis was accompanied by in situ measurement of redox potential (glass probe with Pt electrode and Ag/AgCl (3 M KCl) built-in reference) and pH (glass probe with Ag/AgCl electrode and 3 M KCl). The probes were inserted into the soils to the depth of the mesh bags, avoiding disturbance of Rhizons and mesh bags as much as possible. Redox probes were left in situ overnight to equilibrate before reading. The measurements were corrected according to the measurement of a standard redox buffer (+220 mV; Mettler Toledo, Switzerland), and converted to the standard hydrogen electrode reference (+205 mV for a 3 M KCl Ag/AgCl electrode at 30 °C). Probes for pH measurement were calibrated before use and allowed to equilibrate in situ for >1 h before the pH was read.

2.4. Field incubation experiment

The field experiment was undertaken in a flooded rice paddy during the wet season, from mid-June until mid-October 2021. Due to ongoing projects at the research centre, the profile where the soil was collected was about 150 m from the field experiment location, in the adjacent field. The part of the rice paddy used for the field study was not planted with rice during the experimental season, to exclude the effect of plant roots on the mineral transformation study. Floodwater during the experimental season was supplied by rainfall and additional irrigation water was not required to maintain flooded conditions. The experiment

began approximately two weeks after rice was planted in the other parts of the paddy and was completed before the end of the rice growing season (sixteen weeks in total).

A set of pure and soil-mixed jarosite samples, identical to those used in the mesocosm study, were deployed in the field in topsoils and subsoils at 15 cm and 70 cm depth, respectively. Samples were arranged such that each array contained one set of triplicated samples. Within each array, the corresponding samples from each triplicate were systematically placed to have a different location with reference to one another, porewater sampling points and array boundaries (c.f. array layouts in Fig. S4). Replicate sets of samples were extracted from the field after eight, twelve and sixteen weeks of incubation. Once removed from soil, the samples were immediately sealed under vacuum to limit contact with air. Vacuum sealed sample bags were further sealed in nitrogen-flushed aluminium bags on the same day, and then stored frozen. Once returned to the laboratory, the samples were thawed in a glovebox, then handled as described above for the mesocosm samples.

Porewater was sampled from 15 cm and 70 cm depth on the days when mineral samples were deployed and collected. The porewater was extracted using Rhizons (Rhizosphere research, NL; model 'Macro-Rhizons', 9 cm-long porous filter with 0.15 μm cut-off) which were positioned in the centre of each array of replicate samples on the day when porewater was collected (Fig. S4). Porewater was stored in glass vials, acidified to pH 3–4 with concentrated HCl, and frozen until analysed. The same solution was used for DOC analysis and trace and major element analysis by inductively coupled plasma with mass spectroscopy (ICP-MS; 8800 QQQ, Agilent Technologies). The pH was measured in porewater that was extracted using the same Rhizons using a calibrated glass electrode (3 M KCl Ag/AgCl). Redox measurements were taken with Pt electrodes that were embedded into custom-built 70 cm-long fibreglass probes at intervals of 4–5 cm with an external reference electrode (saturated KCl Ag/AgCl; built by Paleo Terra, NL). Values were recorded after overnight equilibration of the electrodes and converted to the standard hydrogen electrode reference (+194 mV for a saturated KCl Ag/AgCl electrode at 30 °C).

2.5. Analytical methods

Major and trace elemental composition of the porewater solutions was determined by ICP-OES for porewater collected from mesocosms and by ICP-MS for porewater collected in the field. Measurements of DOC in porewater were carried out using a DIMATOC 2000 (Dimatec) total organic carbon analyser. Diluted DOC samples were measured under constant stirring to ensure uptake of any precipitates that formed as a result of freezing and thawing the samples.

The Fe isotopic composition of enriched soils before and after the incubation was measured using ICP-MS analysis of soil extraction solutions. Approximately 150 mg of each ^{57}Fe-jarosite-enriched soil sample was digested in 10 mL of Aqua Regia (8 mL HCl and 2 mL HNO_3) for 90 min at 120 °C (Schulz et al., 2023). Samples were diluted to 100 ppb Fe for isotope analysis and the ICP-MS was operated in H_2-H_2 mode (Schulz et al., 2023). The proportion of the ^{57}Fe attributable to the jarosite enrichment, $^{57}Fe_{Jrs}$, was calculated by comparison to the natural abundance of ^{57}Fe as outlined in Section S6. Data are recorded for each replicate mesh bag in Section S6 and reported as averages of the triplicates in the text.

Powder XRD measurements (D8 Advance, Bruker) were performed on all samples retrieved from pure mineral mesh bags (not ^{57}Fe-jarosite-enriched soil) before and after incubation in soils. Samples were resuspended in ethanol, transferred onto polished Si wafers (711 cut, Sil'tronix Silicon Technologies), and allowed to dry in place. Reacted mineral samples were prepared under anoxic conditions and were closed under anoxic seal during the measurement using an airtight specimen holder with in-built knife to block scattered radiation (Bruker: A100B109). The mineral composition of the samples was determined by Rietveld quantitative phase analysis (QPA) implemented in TOPAS software (Version 5, Bruker) using published crystallographic information files for reference minerals (see Section S7) and an empirically mass-calibrated hkl (PONKCS) phase (Scarlett and Madsen, 2006) for ferrihydrite (ThomasArrigo et al., 2018) based on a previously synthesised 2-line ferrihydrite sample (Grigg et al., 2022). Full details of the measurement, Rietveld fitting routine and reference minerals are provided in Section S7. The results of the Rietveld QPA are presented in the text as the average of triplicates, unless otherwise stated.

The speciation of ^{57}Fe in the solid samples was measured using ^{57}Fe Mössbauer spectroscopy. This spectroscopy is only sensitive to ^{57}Fe in a sample and provides information about the nuclear state of the atom, which may be influenced by the chemical bonding environment and therefore provides information about speciation (Byrne and Kappler, 2019). Mössbauer spectroscopy was performed on soils before and after ^{57}Fe-jarosite enrichment, on a large selection of replicates retrieved from the ^{57}Fe-jarosite-enriched soil mesh bags following incubation, and in parallel to XRD analysis on a small selection of samples retrieved from pure mineral mesh bags following incubation. In ^{57}Fe-enriched soils, Mössbauer analysis was used to trace the reaction pathways of the synthetic minerals. In non-^{57}Fe-enriched soils, Mössbauer spectroscopy was used to characterise ^{NA}Fe mineral phases and to identify XRD-amorphous phases. All samples were measured at 5 K and 77 K. Details of Mössbauer measurements, spectral fitting and phase interpretation are provided in Section S8.1. A summary of the phases that were fit in Mössbauer spectra, including the abbreviations used in the text, is provided in Table 1.

3. Results

3.1. Laboratory mesocosm

3.1.1. Geochemical conditions in laboratory mesocosms

Following the initial flooding of topsoils in laboratory mesocosms, electron acceptors were rapidly consumed by microbial metabolic activity. The Eh decreased from +238 ± 31 mV to –33 ± 18 mV within one week and decreased to −193 ± 10 mV by the end of the experiment, corresponding to an increase of the pH from 4.6 to 6.5 (all errors are 1 standard deviation of the mean of measurements in replicate mesocosms, 1σ; Fig. 1). Therefore, the conditions for microbial Fe reduction, that is, Eh less than approximately +100 mV to +200 mV, depending on the Fe speciation (Lacroix et al., 2023; Reddy et al., 1986), were established within one week of flooding, allowing for Fe(II) to be released into porewater. The Fe concentration peaked at 4.2 ± 0.5 mM after two weeks and gradually declined until the end of the experiment when the concentration was 1.2 ± 0.1 mM (Fig. 1). In subsoils, the chemical changes in the soil were less pronounced, indicating that the microbial metabolic activity was lower. The pH was stable at 3.7 throughout the experiment, and the Eh decreased from +635 ± 34 mV to a minimum of +130 ± 84 mV after two weeks (Fig. 1). Despite the higher Fe content of subsoils compared with topsoils (Table S1), the increase of the porewater Fe concentration in flooded subsoil mesocosms was slower than in topsoils mesocosms, reaching a maximum of 0.6 ± 0.1 mM at the sixteen-week timepoint (Fig. 1).

3.1.2. Laboratory mesocosm incubation of mesh bags containing pure unsubstituted and Al-substituted jarosite

The amount of jarosite remaining in pure-mineral mesh bags incubated in mesocosms occurred in the order: Unsubstituted jarosite in topsoil < Al-jarosite in topsoil < unsubstituted jarosite in subsoil < Al-jarosite in subsoil. The amount of jarosite remaining in the sample is indicative of the amount of jarosite transformation, although the transformation may be underestimated if aqueous Fe was lost from the mesh bags during the incubation. The XRD analysis shows that jarosite in topsoil quickly transformed into goethite, whereas jarosite remained dominant in subsoil incubations throughout the sixteen weeks (Fig. 2A-D). All fits of XRD patterns included a PONKCS phase calibrated to 2-line

Table 1
Summary of components that were fit in Mössbauer spectra in this study. Each phase is presented alongside typical centre shift (CS), quadrupole shift or quadrupole splitting (QS or ε for doublets or sextets, respectively) and hyperfine field (H) parameters, which were used to identify the phases in the fitted Mössbauer spectra. 'Temp' refers to the temperature at which the reference Mössbauer spectral parameters were collected. The phase abbreviations (D1 to D5 and S1 to S5) are used to identify these phases throughout the text. Details about the interpretation are provided in Section S8 (Supplementary material). [a] Average reported when reference spectrum was fit with multiple components.

Fit component	Assigned colour	Interpretation	Typical parameters				
			CS (mm/s)	QS or ε (mm/s)	H (T)	Temp (K)	Ref.
D1 (doublet)		Fe(III), doublet at 77 K: jarosite above blocking temperature.	0.48	1.21	N/A	77	Grigg et al. (2024b)
D2a (doublet)		Fe(II), doublet at 5 K or 77 K: Adsorbed Fe(II) or Fe (II) in ferrous or mixed-valent minerals including phyllosilicates.	1.15–1.42	2.53–3.01	N/A	5	Chen and Thompson (2018, 2021); Notini et al. (2023); Winkler et al. (2018)
			1.09–1.28	2.32–3.0	N/A	77	Chen et al. (2017); Winkler et al. (2018)
D2b (doublet)		Fe(II), doublet at 5 K and 77 K: interpreted as possibly part of green-rust-like mineral in association with Sextet S4.	1.35	3.2	N/A	5	Cuttler et al. (1990)
D3 (doublet)		Fe(III), doublet at 5 K and 77 K: Fe(III) in phyllosilicate clays or organic complexes.	0.47–0.52	0.54–0.73	N/A	77	Chen and Thompson (2021); Lee et al. (2012); Winkler et al. (2018)
			0.46–0.49	0.60–0.79	N/A	4.2 or 5	Chen and Thompson (2021); Notini et al. (2023); Winkler et al. (2018)
			0.5	0.5 – 0.8	N/A	77	OM-Fe(III): Goodman et al. (1991)
D4 (singlet)		Fe(II), singlet at 5 K and 77 K: stoichiometric mackinawite.	0.49–0.51	0	N/A	5	Schröder et al. (2020)
D5 (doublet)		Fe(III), doublet at 77 K but not at 5 K: possibly poorly crystalline Fe oxyhydroxides.	–	–	N/A	77	No precedent
S1 (sextet)		Fe(III), sextet at 5 K; jarosite below blocking temperature.	0.49	−0.07	48.4	5	Grigg et al. (2024b)
S2 (sextet)		Fe(III), sextet at 5 K and 77 K: Fe oxyhydroxides, mostly goethite and ferrihydrite. Contains rather more goethite than ferrihydrite, or goethite with higher crystallinity and purity, when fitted ε and H are higher.	0.47–0.49	−0.08–−0.15	49.4 – 50.6	4.2 or 5	Gt: Notini et al. (2022); Wan et al. (2017)
			0.46–0.48	0.00–−0.03	48.4–49.1[a]	5	2-line Fh: Byrne and Kappler (2022); Schulz et al. (2023); ThomasArrigo et al. (2017)
			Not reported	Not reported	48.5	5	nm-Al-Gt: Murad and Schwertmann (1983)
S3 (sextet)		Fe(II), sextet at 5 K: FeS_x	0.48	−0.02	27.8	4.2	Wan et al. (2017)
			0.10–0.85	−0.2–0.08	7.4–20.2	5	Thiel et al. (2019)
S4 (sextet)		Fe(III), sextet at 5 K with large σ_H: possibly part of green-rust-like mineral in association with doublet D2b.	0.47	−0.2	50.4	5	Cuttler et al. (1990)
S5 (sextet)		Collapsed feature	N/A	N/A	N/A	N/A	N/A

ferrihydrite (reported in Table S8 and S9 and plotted in Fig. 2A-D). However, the presence of ferrihydrite cannot be confirmed by XRD analysis due to the limitations on the quantification of XRD-amorphous phases (explained in Section S7.1) and small quantities of ferrihydrite (<15 %) in the XRD QPA. The fitted ferrihydrite contributions were between 5 % and 15 % and were not likely to have impacted the interpretation of the relative abundance of the other fitted phases. Mössbauer spectra of sixteen-week samples from all four treatments (that is, unsubstituted and Al-jarosite in topsoil and subsoil) were predominantly consistent with mixtures of jarosite and goethite with minor amounts of additional minerals including ferrihydrite (Fig. S15).

When unsubstituted jarosite was incubated in topsoil mesocosms, complete transformation was observed within sixteen weeks with goethite as the dominant product phase in the XRD QPA (Fig. 2). Jarosite was not identified in the XRD patterns after 16 weeks (Fig. S7). Likewise, Mössbauer spectra were dominated by a sextet with quadrupole shift (ε) of −0.12 mm/s and hyperfine field (H) of 49.7 T at 5 K, consistent with goethite and occupying 86 % of the sample (Table S10; c.f. phase S2 in Table 1). Although a minor phase with parameters matching initial unsubstituted jarosite was fit (Table S10), the Mössbauer features of jarosite were not individually identifiable by characteristic peaks (Fig. S15), and therefore the jarosite content may have been overestimated. An additional minor phase, without clear peaks and fitted as a collapsed feature at 5 K, presents as a ferrous doublet at 77 K with centre shift (CS) of 1.06 mm/s and quadrupole splitting (QS) of 2.90 mm/s (Table S10; c.f. phase D2a in Table 1), indicating the presence of a poorly or non-crystalline Fe(II)-bearing phase.

The transformation of Al-jarosite proceeded more slowly than unsubstituted jarosite in topsoil mesocosms, and more poorly crystalline and XRD-amorphous phases were formed. After sixteen weeks, Al-jarosite contributed to 45 % of the XRD QPA (Fig. 2B) and 46 % of the Mössbauer spectrum collected at 5 K (Table S10). The dominant product was goethite, comprising 43 % of the fitted XRD pattern (Fig. 2B). Correspondingly, 44 % of the Mössbauer spectrum collected at 5 K was fit as phase S2 with ε = −0.12 mm/s and H = 49.2 T likely indicating that the phase was dominated by goethite (Table S10, c.f. phase S2 in Table 1). Ferrihydrite could not be uniquely identified in the Mössbauer spectra, but may form part of phase S2. Two minor phases were also identified. Phase S3, with CS = 0.17 mm/s and H = 11.4 T, was fit in spectra collected at 5 K, consistent with metastable Fe sulfides, denoted as FeS_x where X>1 (Table S10, c.f. phase S3 in Table 1). A further part of the Mössbauer 5-K spectral area was identified as phase D2b, potentially consistent with a green-rust like mineral (Cuttler et al., 1990).

In subsoils, jarosite remained the dominant phase during the incubations. Unsubstituted jarosite accounted for 85 % of the XRD patterns following sixteen weeks of incubation (Fig. 2C) along with 3 %

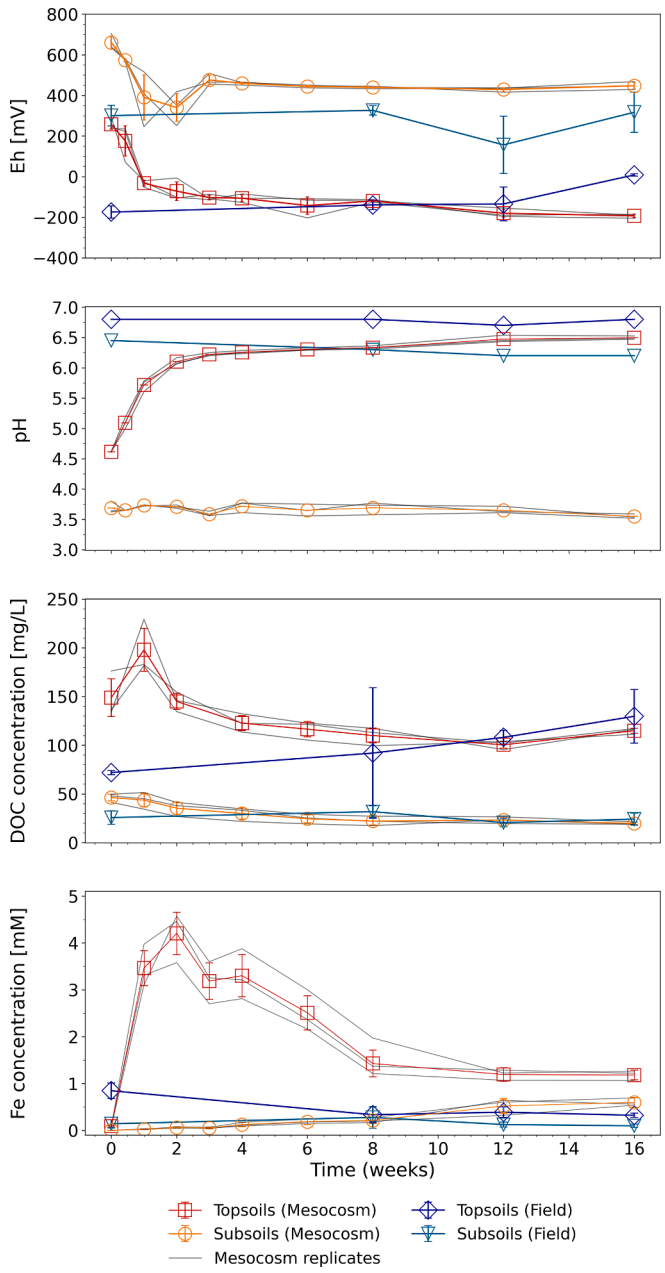

Fig. 1. Time series plot of soil properties in laboratory microcosms and field sites. Error bars indicate 1σ of measurements of samples from triplicate mesocosm reactors (duplicate samples from triplicate mesocosms for Fe concentration). Panel A plots the Eh measured in situ in the soil, Panel B plots pH measured in situ, Panel C plots DOC measured in porewater (error bars on coloured plots indicate 1σ of measurement replicates) and Panel D plots the concentrations of Fe in porewater measured by ICP-OES.

goethite and a PONKCS ferrihydrite phase (Table S8). Similarly, in Al-jarosite incubations, the Al-jarosite was the only crystalline mineral identified in the XRD patterns, but a PONKCS ferrihydrite phase was also included in the fit (Fig. 2D). In Mössbauer spectra, the initial unsubstituted jarosite phase contributed to 57 % of the 5-K spectrum of 16-week incubated samples, while the Al-jarosite occupied 74 % of the spectrum at 5 K (Table S10). Phase S2 in 5-K spectra, corresponding to phase D5 in 77-K spectra, is likely due to short-range-ordered (SRO) Fe oxyhydroxides. Phase S2 in spectra measured at 5 K ($\varepsilon = -0.06$ and H = 48.2) was consistent with the presence of ferrihydrite (Byrne and Kappler, 2022; Schulz et al., 2023; ThomasArrigo et al., 2017). A small area was fit as phase S2 in Al-jarosite treatments ($\varepsilon = -0.08$ and H = 47.0), likely also consistent with ferrihydrite (Byrne and Kappler, 2022; Schulz et al., 2023; ThomasArrigo et al., 2017) or nano-crystalline Al-goethite that magnetically orders below 77 K (Murad and Schwertmann, 1983). The 5-K Mössbauer spectrum from Al-jarosite treatments contained a ferrous doublet and a sextet, which have been assigned the phases D2b and S4, as they resemble the phases observed in the Al-jarosite incubation in topsoil. In contrast, disordered transformation products were not detected in unsubstituted-jarosite treatments (Fig. S15).

3.1.3. *Laboratory mesocosm incubation of mesh bags containing ^{57}Fe-jarosite-enriched soil*

As in pure-mineral mesh bags, jarosite with and without Al-substitution occurred as a diminishing fraction of the Fe minerals in the incubated jarosite-enriched soils. After 16 weeks of incubation, unsubstituted jarosite and Al-jarosite explained 14 % and 13 % of the ^{57}Fe, respectively, in samples from topsoil mesocosms measured by Mössbauer spectrometry at 77 K (mean of triplicates; Fig. 4 and Table S12). In 16-week incubated subsoils, 46 % and 61 % of the ^{57}Fe in the 77-K spectra occurred as unsubstituted jarosite and Al-jarosite, respectively (mean of triplicates; Fig. 4 and Table S12). The ^{57}Fe phases in the samples following the incubation were dominated by poorly crystalline or non-crystalline phases.

Among the mineral phases in the Mössbauer spectra of all jarosite-enriched soil samples after incubation, two ferric phases were identified: phase D3, which presented as a doublet at 5 K, and phase S2, which presented as a sextet at 5 K (Table 1). Phase D3 had CS between 0.34 and 0.54 mm/s and QS between 0.38 and 0.76 mm/s in all treatments after sixteen weeks (5-K spectra; Table S12), which was similar to the CS of 0.46 mm/s and QS of 0.53 to 0.55 mm/s that were fit in the Fe(III) doublet in the initial soil before ^{57}Fe-jarosite enrichment (Table S11). The variation in the fitting parameters of phase D3 indicates that some composition changes in this phase may have occurred during the incubation. Phase S2 was predominantly found in subsoils and was not identified or occupied < 10 % of the total spectral area in topsoils after sixteen weeks of incubation. In subsoils, phase S2 had ε between −0.06 and −0.14 mm/s and H > 49.3 T in most samples at 5 K, consistent with goethite or 6-line ferrihydrite (Table S12, c.f. Table 1). The sextet was more prominent in unsubstituted jarosite-enriched subsoil (26 % of spectral area in sixteen-week incubated samples; Table S12) than in Al-jarosite-enriched subsoil (only identified in one triplicate at 5 K in sixteen-week incubated samples; Table S12). There was no consistent difference between the size of the sextet at 5 K and 77 K that would have indicated the presence of a phase that ordered between those temperatures, such as 2-line ferrihydrite.

Ferrous phases were also a major component of Mössbauer spectra from jarosite-enriched topsoils and present in some jarosite-enriched subsoils. The spectra collected at 77 K were dominated by a ferrous doublet, identified as phase D2a (see Table 1), which increased in area throughout the incubation and reached up to 53 % of the total ^{57}Fe in all jarosite-enriched topsoils after sixteen weeks (compare Fig. 3A with Fig. 3C and Fig. 3F). At 5 K, the size of phase D2a was smaller and was compensated by the occurrence of phase S5. Phase S5 showed properties similar to a ferrous phase previously observed in incubated paddy soils that was attributed to Fe(II) sorbed to magnetically ordered Fe(III) phases (Winkler et al., 2018). In some replicates, peaks that may have been associated with an octet could be identified, but limitations with the full static Hamiltonian (FSH) fitting routine, interaction with other spectral peaks and poor crystallinity prevented the identification and quantification of a ferrous mineral phase. The proportion that remained as phase D2a at 5 K in topsoils had CS = ~1.3 and QS = 2.86–3.05 and 2.90–2.92 mm/s for jarosite and Al-jarosite, respectively (Table S12), consistent with Fe(II) that is sorbed to solid phases without long-range crystal ordering, or in phyllosilicates (Chen et al., 2017; Notini et al., 2023; Winkler et al., 2018).

The jarosite transformation must be analysed within the context of a changing isotopic composition of the sample during the experiment

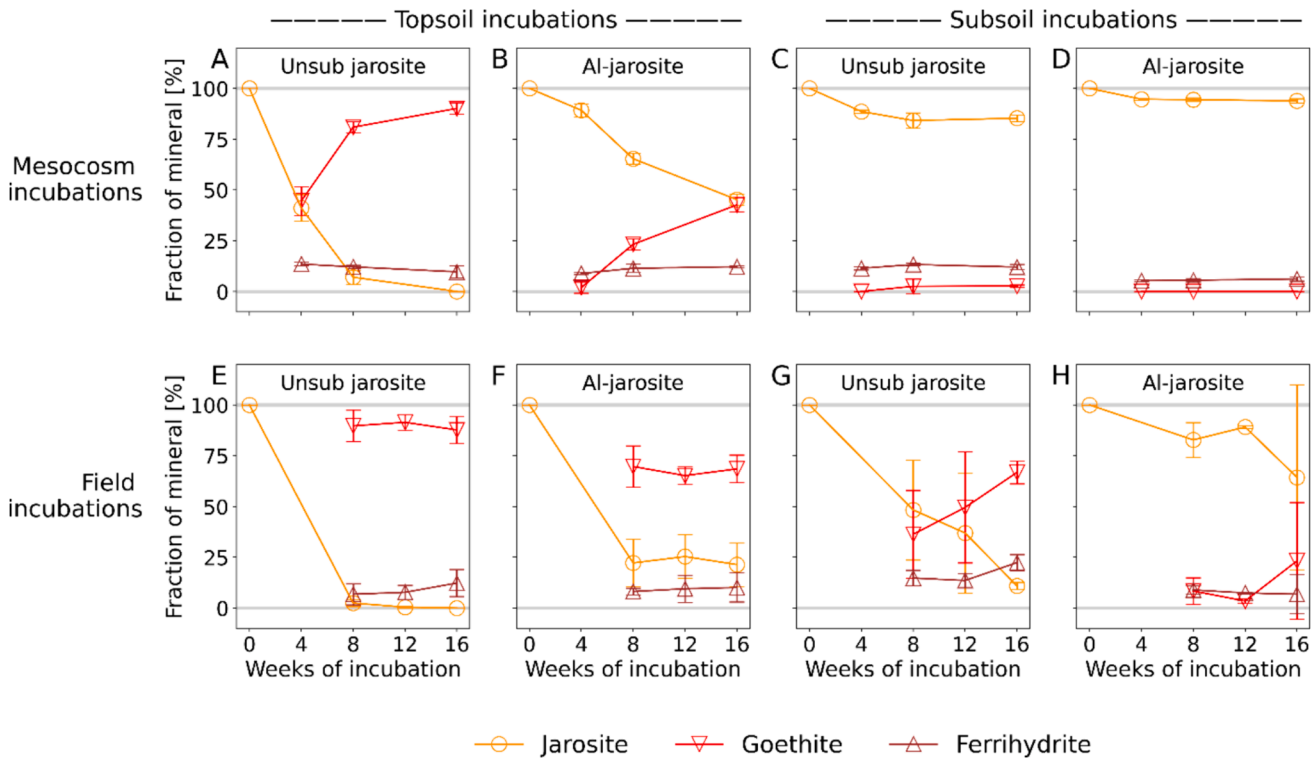

Fig. 2. Plot of mineral composition in pure-mineral mesh bags over time, quantified by Rietveld analysis of XRD patterns. All data points are averages of samples from triplicate laboratory mesocosms or triplicate field sample arrays, with error bars indicating one standard deviation of the mean. The top row contains plots of minerals incubated in the laboratory mesocosms, while the bottom row contains plots of minerals incubated in the field. From left to right, plots show unsubstituted jarosite incubated in topsoil (Panels A and E), Al-jarosite incubated in topsoil (Panels B and F), unsubstituted jarosite incubated in subsoil (Panels C and G), Al-jarosite incubated in subsoil (Panels D and H). Minor amounts of lepidocrocite and mackinawite that were detected in isolated replicates were excluded from the chart. The mackinawite detected in one replicate explains why the total mineral fractions at week sixteen in Panel H are less than 100 %. All mineral fractions from Rietveld QPA are presented in Table S8 and S9 and plots of XRD patterns are shown in Fig. S6–S14.

(Section S6). The measured contribution of ^{57}Fe from the mineral spike decreased from 96 % to 38 % and 47 % for unsubstituted and Al-jarosite in topsoil, respectively, and from 95 % to 85 % and 91 % for unsubstituted and Al-jarosite in subsoil, respectively, over the sixteen weeks (Fig. 4 and Section S6). The change in the isotopic composition indicates that ^{57}Fe was lost from the mesh bags during the incubation by dissolution of the jarosite and transport of dissolved Fe through the mesh, similar to the process observed in Schulz et al. (2023). However, the amount of ^{57}Fe loss from the mesh bag that would have been necessary to cause the observed shifts in the isotopic ratio was greater than the observed change in the total Fe content of the samples (Table S7). The difference indicated that some aqueous ^{NA}Fe from the soil porewater likely also entered the mesh bags during the incubation. The loss of ^{57}Fe from the mineral spike in the mesh bags would have increased the prominence of ^{57}Fe in the minerals from the natural soil minerals in the Mössbauer spectra. Furthermore, a fraction of ^{57}Fe in the samples can be attributed to the natural ^{57}Fe content of the reduced Fe in porewater that formed mineral phases inside the mesh bag.

3.2. Field experiment

3.2.1. Geochemical conditions in the field

The geochemical conditions in field soils were more stable throughout the experiment than those measured in laboratory mesocosms. Since sample deployment did not coincide with the initial flooding of soils, reducing conditions had established in the rice paddy topsoil once the experiment began, and the conditions prevailed throughout the experiment (Fig. S5). In topsoils, the Eh was −175 ± 30 mV at the beginning of the experiment, rising in the last four weeks to +8 ± 6 mV (Fig. 1 and Fig. S5). The pH was 6.8 at the beginning and remained stable (Fig. 1). The Fe concentration in the topsoil was 0.8 ± 0.2 mM at week zero, which was lower than the peak concentrations observed in topsoil mesocosms and fell to 0.3 ± 0.05 mM during the experiment (Fig. 1). In subsoils, the redox conditions were established before the beginning of the experiment. The average Eh in the subsoils varied between +157 mV and +327 mV during the experiment, without a discernible trend over time. While pH started at 6.5 and fell to 6.2 by week 16 the pH remained higher than the pH observed in mesocosms containing subsoil (Fig. 1 and Fig. S5). The Fe concentration in porewater was 0.1 ± 0.1 mM throughout the experiment (Fig. 1).

3.2.2. Field incubation of mesh bags containing pure unsubstituted and Al-substituted jarosite

Jarosite in pure-mineral mesh bags incubated in the field followed a pattern of transformation similar to that observed in the mesocosms, whereby fractions of remaining jarosite (untransformed, data from XRD) after sixteen weeks increased in the order: unsubstituted jarosite in topsoil < Al-jarosite in topsoil < unsubstituted jarosite in subsoil < Al-jarosite in subsoil. As in the mesocosms, the XRD and Mössbauer analysis showed that jarosite was progressively replaced by goethite, while some treatments contained poorly crystalline and/or XRD-amorphous phases, including possible ferrihydrite. Larger variation can be observed between replicates that were incubated in the field compared with replicates in the mesocosms. The standard deviation (1σ) among triplicate measurements of jarosite mineral proportion at each timepoint was as high as 6.6 in the laboratory mesocosms (average 1σ was 2.7), but up to 45.5 in the field (average 1σ was 12.1; cf. error bars in Fig. 2).

In topsoils, the transformation of unsubstituted jarosite proceeded with comparable rates and products as measured in the mesocosms. Jarosite was not observed in XRD patterns after eight weeks and the

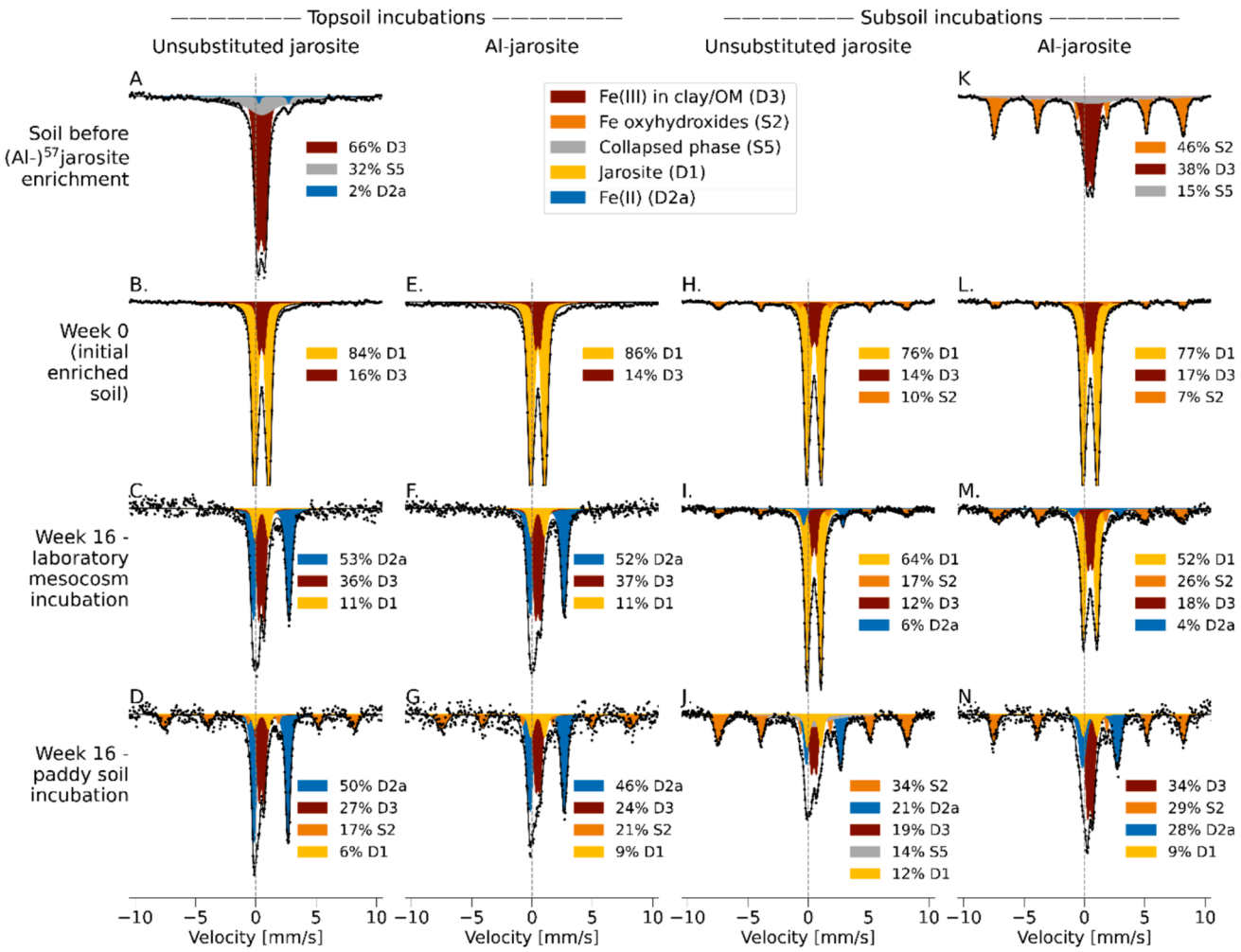

Fig. 3. Comparison plot of Mössbauer spectra, collected at 77 K, from original soil (top row), original soil-mineral mix (second row), sixteen-week incubation in the laboratory mesocosms (third row) and sixteen-week incubation in the field (fourth row). Columns show spectra of unsubstituted jarosite in topsoil, Al-jarosite in topsoil, unsubstituted jarosite in subsoil and Al-jarosite in subsoil, respectively. All spectra are normalised by the total fitted area. Only one replicate is plotted in this figure. Plots of all replicates are found in Fig. S16–S23. Fitted phases are identified as jarosite where the mineral phase identification is clear, or as numbered phases which are identified in Table 1. All fitting data and phase interpretation is presented in Tables S12 and S13.

patterns collected after sixteen weeks were predominantly fit as goethite (Table S9). Correspondingly, over 80 % of the 5-K and 77-K Mössbauer spectra of combined replicates was fit as phase S2 with $\varepsilon = -0.12$ mm/s, consistent with goethite (Table S13). A collapsed feature accounted for approximately 10 % and 14 % of the 5-K and 77-K spectral areas, respectively (Table S10).

Aluminium-jarosite transformation in topsoil was initially faster in the field than in mesocosms, but remaining Al-jarosite after sixteen weeks was similar in both of the experiments. After sixteen weeks in topsoil, Al-jarosite was almost entirely transformed and XRD patterns were fit as 70 % goethite, with a ferrihydrite PONKCS phase included in the fit (Fig. 2F and Table S9). The Mössbauer spectrum of combined replicates after sixteen weeks was explained by the initial Al-jarosite phase (27 % at 5 K) and phase S2 (46 % at 5 K), with ε of −0.12 mm/s and H of 49.4 T, predominantly consistent with goethite or 6-line ferrihydrite (c.f. Table 1 and Table S10). As in the mesocosm incubation of Al-jarosite in topsoil, other minor phases that were observed in the Mössbauer spectra were fit as a broad collapsed feature (Fig. S15).

In subsoils in the field, unsubstituted jarosite transformed more quickly than in subsoil mesocosms. Jarosite accounted for 10 % of the XRD patterns after sixteen weeks (Fig. 2G and Table S9), with the remainder predominantly fit as goethite. Mössbauer spectroscopy was not measured on this treatment due to the limited amount of sample material. In contrast, the transformation of Al-jarosite occurred at a similar rate in field and mesocosms subsoils, except for a strong deviation from the trend in a single replicate from the field. Al-jarosite accounted for more than 92 % of the XRD-detectable mineral fraction in two replicates from the field, consistent with the trend of slow transformation observed after eight and twelve weeks (Fig. 2H and Table S9). Likewise, 5-K Mössbauer spectra collected from the replicate that was incubated in array 1 contained mostly jarosite but also contained SRO Fe oxyhydroxides such as 2-line ferrihydrite, which was observed as phase S2 with ε of −0.08 mm/s and H of 48.2 T at 5 K, and phase D5 at 77 K (c.f. Table 1 and Table S10).

In contrast to the trends observed in all other samples, one replicate of the Al-jarosite that was incubated in subsoil for sixteen weeks (from array 2 in Fig. S3) contained 0 % jarosite in XRD patterns, and was replaced by 64 % goethite, 20 % XRD-amorphous mineral that was fit using the 2-line ferrihydrite PONKCS phase and 13 % mackinawite (Table S9). The Mössbauer spectra of the sample contained a singlet at both 5 K and 77 K (phase D4, 10 % of spectral area at 5 K, Table S11), consistent with stoichiometric mackinawite (Schröder et al., 2020). The rest of the Mössbauer spectra were dominated by ferric phases, including phase S2 with $\varepsilon = -0.13$ mm/s at 5 K, consistent with goethite, and phase D3 (data in Table S10 and phase interpretation in Table 1). The presence of pyrite in the Mössbauer spectra cannot be ruled out, but

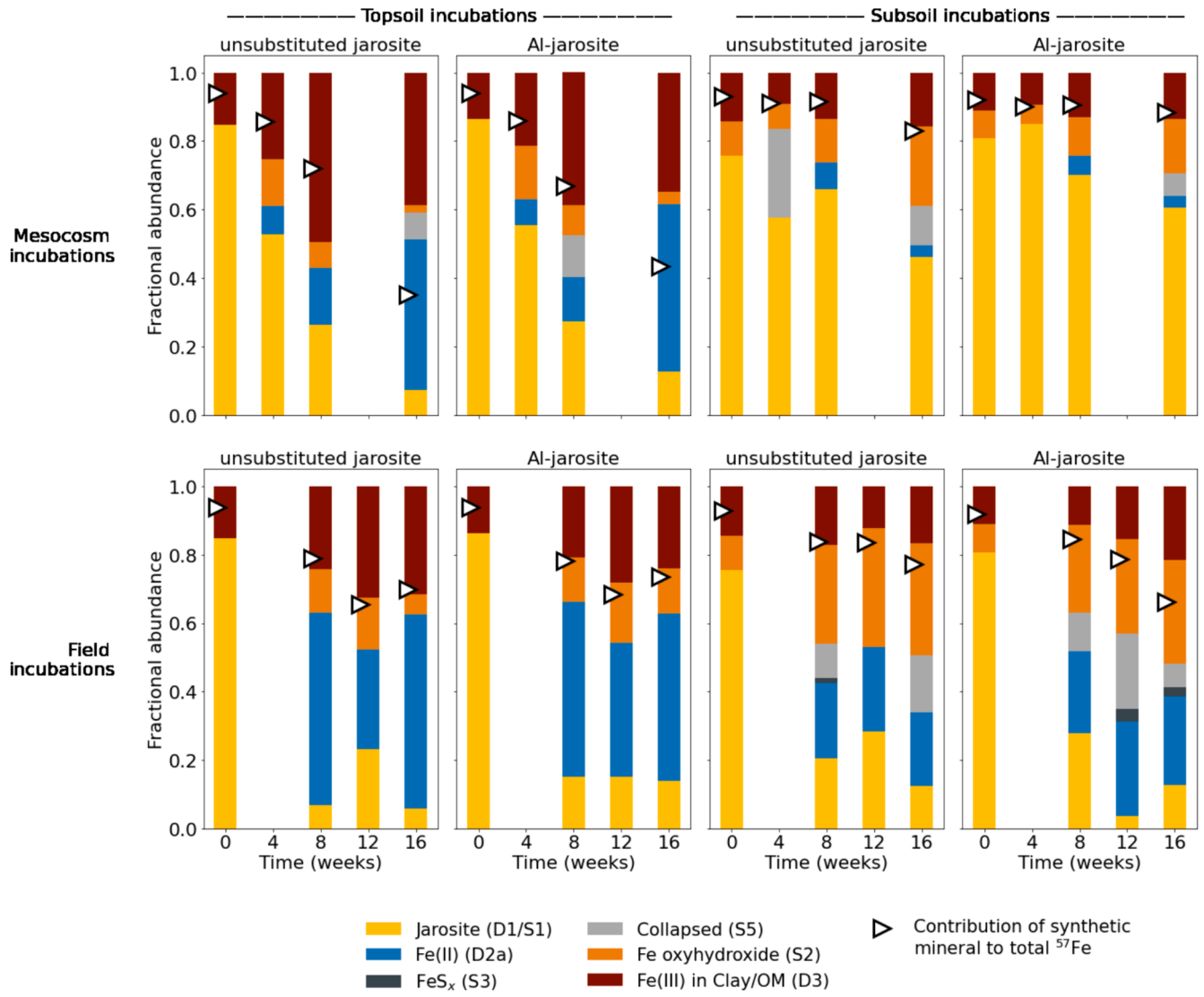

Fig. 4. Timeseries of unsubstituted jarosite and Al-jarosite fitted in Mössbauer spectra collected at 77 K from laboratory microcosms (top row) and field systems (bottom row). Solid filled bars indicate the proportion of each phase fit in the Mössbauer spectra. Cool (blue/grey) colours represent the reduced Fe phases and warm (red/yellow) colours represent the oxidised Fe phases. The triangle markers indicate the proportion of the ^{57}Fe that may be attributed to the synthetic mineral enrichment (below the marker) or background soil (above the marker) based on the ^{57}Fe abundance in digested soil samples. The plotted values are averaged across replicates (error bars not indicated). Variability between replicates is illustrated in Fig. S25, which is a plot of all measured replicates. Data from 5-K measurements are plotted in Fig. S24.

pyrite normally presents a larger QS (approx. 0.6 mm/s) than the doublets measured in these spectra (Ruecker et al., 2016; Wan et al., 2017).

3.2.3. *Field incubation of mesh bags containing ^{57}Fe-jarosite-enriched soil*

As in the mesocosms, Mössbauer measurements of jarosite-enriched soil that were incubated in the field indicated that the amount of ^{57}Fe present as jarosite decreased with time, suggesting that jarosite transformation was occurring during the field incubations. Although some jarosite was fit in the 77-K Mössbauer spectra from all treatments at each timepoint, there is no evidence of a jarosite sextet in the 5-K spectra of samples collected from topsoils enriched in unsubstituted jarosite after eight, twelve or sixteen weeks or enriched in Al-jarosite after sixteen weeks (Figs. S20 and S21). After sixteen weeks of incubation, jarosite explained 9 % of the 5-K Mössbauer spectra from unsubstituted-jarosite-enriched subsoils (average of triplicates listed in Table S13) and was only fit as a minor phase in one replicate of Al-jarosite-enriched subsoil.

An increase in ferric phases other than jarosite was observed in all field-incubated samples. As in the mesocosms, there was an increase in the area fit by phase D3 (see interpretation in Table 1). Sextet S2 was also a feature of Mössbauer spectra from ^{57}Fe-enriched soils that were incubated in topsoils and subsoils in the field. In spectra of sixteen-week incubated soils collected at 5 K, almost all sextets S2 had ε between −0.09 and −0.12 mm/s and H above 49.3 T (Table S13), which was largely consistent with goethite (Notini et al., 2022; Wan et al., 2017) or 6-line ferrihydrite (Byrne and Kappler, 2022) but may also contain some 2-line ferrihydrite, especially in samples with large difference in the area of phase S2 at 77 K and 5 K. The size of this phase S2 was larger in field-incubated samples than mesocosm-incubated samples, was largest in the subsoil, and grew more quickly than phase D3 over the course of the sixteen weeks.

Iron(II) phases also formed a significant fraction of the ^{57}Fe in the jarosite-enriched soil incubated in both field topsoil and field subsoil. Phase S3, interpreted as FeS_x (see Table 1 and Section S8.1), was observed in some replicates from Al-jarosite-enriched subsoil (area up to 6 %; Table S13). Furthermore, as in mesocosm topsoils, phase D2a was fit in 77-K Mössbauer spectra, accounting for 29–68 % of ^{57}Fe in individual replicates from subsoils (Table S13; compare Fig. 3A with Fig. 3J and Fig. 3N) and 17–31 % of ^{57}Fe in individual replicates from topsoils

(Table S13; compare Fig. 3A with Fig. 3D and Fig. 3G). Some of the area of phase D2 in 77-K spectra was transferred to a collapsed feature (phase S5) in 5-K spectra.

As in the mesocosms, the change in the mineralogy over the sixteen-week incubation may be partially explained by the loss of ^{57}Fe from the mesh bag by dissolution of the spiked jarosite and diffusive or convective transport out of the mesh bag and by ingress of ^{NA}Fe from soil into the mesh bags (Table S5 and S6). Based on the measurement of the isotopic ratios in the solution, the contribution of the initial mineral spike to the total ^{57}Fe content of the jarosite-enriched soils was calculated to have decreased from 96 % to 72 % and 76 % for unsubstituted and Al-substituted jarosite in topsoil, respectively and from 95 % to 87 % and 69 % for unsubstituted and Al-substituted jarosite in subsoil, respectively (Fig. 4 and data tables in Section S6).

4. Discussion

4.1. Porewater geochemistry influences the rate and products of jarosite transformation

The mineral transformations that occurred in pure-mineral mesh bags provide a direct indication of the effect of the porewater geochemistry on the transformation of minerals, since the synthetic minerals in pure-mineral mesh bags were exposed to porewater that formed in the soil without being mixed with the solid matrix. Jarosite transformed more quickly when exposed to porewater from topsoils than porewater from subsoils in both laboratory mesocosm and field incubations. Several differences in the geochemistry of topsoils and subsoils could have contributed to the different rates of transformation. Notably, topsoils were strongly redox active, with an Eh within the range of Fe reduction within approximately one week in mesocosms, and throughout the experiment in the field (Fig. 1). Jarosite transformation is accelerated under reducing conditions, when Fe(III) in mineral phases such as jarosite may be reduced and dissolved (Kölbl et al., 2022; Kölbl et al., 2021). The onset and maintenance of reducing conditions in soils likely depended on the amount of microbial metabolism that could be sustained by the availability of organic matter in the soil (Kölbl et al., 2022; Kölbl et al., 2021). Indeed, in our incubations, the higher DOC observed in topsoils compared with subsoils was associated with lower Eh in topsoils (Fig. 1). However, the transformation is also affected by other geochemical changes that occur as the result of microbial metabolism and the onset of reducing conditions.

The pH of the porewater was likely an important factor in the rate of jarosite transformation in soil. In subsoil mesocosms, little jarosite transformation was observed over sixteen weeks. The pH in subsoil (3.5 at week 16) was analogous to studies of jarosite in mixed suspensions under acidic conditions, in which jarosite did not undergo any Fe(II)-catalysed transformation within 24 h (pH 4.0, Karimian et al., 2018). Longer-term mixed suspension studies have not been undertaken at this pH, preventing a direct comparison of the transformation rates at low pH over four months. In contrast, the elevated pH of the topsoil in mesocosms (6.5 by week 16) and the field (average 6.8 throughout the experiment) may have promoted jarosite dissolution (Trueman et al., 2020) and was consistent with a higher rate of Fe(II)-catalysed jarosite transformation at circumneutral pH (Karimian et al., 2017, 2018). In the field, the pH of the subsoil porewater was also significantly higher (average pH of 6.3 throughout the experiment) than the pH of porewater collected from subsoil mesocosms, which could have contributed to the faster rate of jarosite transformation in subsoils from the field compared to subsoils from the laboratory mesocosms.

The reductive dissolution of Fe minerals under low Eh conditions led to the higher concentration of Fe(II) in porewater from topsoils compared to subsoils. The higher Fe(II) concentration in porewater from topsoil may have been another factor that accelerated the rate of jarosite transformation. However, the transformation of unsubstituted and Al-jarosite in both topsoil and subsoil was slower than observed in well-mixed mineral suspension experiments. For example, synthetic unsubstituted- and Al-jarosite samples, equivalent to those used in this soil incubation study, were previously observed to transform completely within 2–8 h when reacted as a well-mixed suspension in a circumneutral anoxic Fe(II) solution (Grigg et al., 2024a). The well-mixed suspension contained Fe(II) concentrations of 5 mM, similar to the maximum Fe(II) concentration of 4.2 mM in the porewater from topsoils in the laboratory mesocosms in this study (Fig. 1; Grigg et al., 2024a). The slower transformation of jarosite is consistent with a previous study that measured jarosite transformation to goethite over the course of a year under the influence of a chemically complex porewater matrix in a creek sediment (Vithana et al., 2015).

It is possible that the slower transformation of jarosite was caused by limited diffusion of Fe(II) into the mesh bags, and interactions between the jarosite and other ions that simultaneously diffused into the mesh bags. Iron diffusion is required for Fe(II)-catalysed transformation processes, as the lack of electron donors in the mesh bags likely limited the in situ biologically driven reductive dissolution of Fe. In soil, precipitation of Fe(II) minerals may have limited the Fe(II) available to diffuse into the mesh bags. Furthermore, the pH and Eh of subsoils suggest that some oxidation of Fe(II) could have occurred, especially in oxic microsites. Slower transformation of pure Fe minerals in soil incubations using mesh bags has been previously observed in the case of ferrihydrite, where diffusion limitations of Fe(II) from soil surrounding the mesh bag slowed the rate of mineral transformation in the core of the mesh bag (Grigg et al., 2022). Mesh bags used in this study contained a fifth (w/w) as much mineral as mesh bags from the ferrihydrite study (Grigg et al., 2022) to minimise the effect of Fe(II) diffusion on the jarosite transformation rate. The transformation of ferrihydrite in soil has also demonstrated that Fe(II)-catalysed transformation processes could be inhibited by the adsorption of compounds such as PO_4, SiO_4 and DOC to the surface binding sites of the minerals in the outer rim of the mesh bag (Grigg et al., 2022). Similarly, sorption of Si and natural organic matter to the surface of jarosite has been shown to inhibit mineral transformation (Jones et al., 2009). Therefore, we expect that sorption of ions to mineral surfaces inhibited the rate of jarosite transformation in this study.

In addition to the rate of jarosite transformation, the transformation products indicate how the porewater from ASS can influence the transformation processes. Goethite was the dominant product of jarosite transformation in pure-mineral mesh bags in both topsoil and subsoil, while some ferrihydrite was present, especially in subsoil incubations (Table S8 and S9). The prevalence of goethite among the transformation products is consistent with long-standing interpretation of pedological processes and Fe cycling in ASS (Van Breemen and Harmsen, 1975). The absence of lepidocrocite among the products of the transformation, apart from traces observed in isolated replicates, contrasted the outcomes of jarosite transformation experiments in mixed-suspensions containing Fe(II) in a pH range from 4 to 7 (Grigg et al., 2024a; Karimian et al., 2017, 2018). The absence could indicate that ions in the porewater impeded lepidocrocite formation. Alternatively, limited Fe(II) diffusion into the mesh bag may have lowered the ratio of Fe(II) to Fe(III) at the mineral surfaces compared to conditions in a well-mixed suspension, which was previously shown to reduce lepidocrocite formation during the Fe(II)-catalysed transformation of ferrihydrite (Hansel et al., 2005). Apart from the Fe oxyhydroxides, crystalline Fe monosulfide (mackinawite) was observed in one replicate of Al-jarosite incubated in subsoil in the field, and small amounts of FeS_x were observed in several pure-mineral and jarosite-enriched soil mesh bags. These isolated occurrences of sulfide minerals demonstrate the importance of geochemical heterogeneity on the sub-metre scale in paddy systems and show that reduced S can increase the transformation rates of jarosite and alter the transformation products of jarosite in soil.

4.2. Soil-mineral contact promotes the formation of poorly crystalline and non-crystalline products following reductive dissolution

In addition to the composition of porewater, the proximity of minerals to other components of the solid matrix may also alter the mineral transformation processes (Schulz et al., 2023). Indeed, the products of transformation differed significantly between incubations of pure minerals and jarosite-enriched soil, offering complementary insight into the stability of jarosite in soil. Since the pure-mineral mesh bags initially contained only jarosite, they simulate the relative mineralogical purity of naturally occurring jarosite mottles in ASS. Therefore, the dominance of Fe(II)-catalysed transformation processes in the pure-mineral mesh bags may indicate that this process is favourable in naturally formed jarosite mottles. However, the mesh bags were not designed to imitate the porosity of natural mottles, and natural mottles could also contain mineralogical impurities (Grigg et al., 2024b), direct interfaces with the soil matrix outside the mottle (Poch et al., 2009; Van Breemen and Harmsen, 1975), and possibly unique bacterial communities (Cahyani et al., 2008). Therefore, mixing of the ^{57}Fe-jarosite with the soil matrix provides an important alternative view of the transformation processes that may occur in the soil, especially at the edges of jarosite mottles, or where jarosite is mixed with other components of the soil matrix.

When synthetic minerals were separated from soil in pure-mineral mesh bags, in both field and laboratory mesocosm experiments, the products of jarosite transformation were largely consistent between XRD and Mössbauer analyses, being dominated by goethite. Mössbauer spectroscopy revealed only small amounts of poorly crystalline and non-crystalline minerals alongside the dominant Fe oxyhydroxides. Firstly, phase D2b and S4, together interpreted as possible green rust (see Section S8.1), were identified in a small number of mesh bags. Secondly, the occurrence of Fe sulfides other than mackinawite in Mössbauer spectra indicate that sulfidation of jarosite was occurring in some samples where mackinawite was not formed. The geochemical conditions of the incubations were measured at one location for each array of sample replicates, and not for individual replicates. Therefore, the porewater measurements could not capture the spatial heterogeneity that corresponded to the formation of either poorly crystalline FeS_x or crystalline mackinawite.

In contrast to the pure-mineral mesh bags, Fe oxyhydroxide products of Fe(II)-catalysed jarosite transformation were not major phases in the Mössbauer fits of incubated soil. The dominance of the ferrous doublet (D2a, Figs. 3 and 4) indicated that reductive dissolution of jarosite led to a release of Fe(II), which was adsorbed to mineral surfaces, was complexed by organic matter, or formed ferrous or mixed-valence minerals in the mesh bag (Chen and Thompson, 2018, 2021; Notini et al., 2023; Winkler et al., 2018). The presence of these phases could indicate that reductive dissolution of Fe(III) in jarosite was the dominant process of jarosite transformation in topsoil mesocosms and all field soils. The bio-reduction of Fe(III) within the jarosite structure may have been mediated by Fe-reducing bacteria (Jones et al., 2006) when jarosite was incubated with direct contact to the soil matrix. Although aqueous Fe(II) catalyses the transformation of Fe minerals, including jarosite, to secondary products, such as Fe oxyhydroxides, by a process of oxidation of Fe(II) at the jarosite mineral surface and with reduction of Fe(III) from the jarosite structure (Grigg et al., 2024a), the products of this transformation were not major phases in the Mössbauer spectra. The porewater from topsoils and subsoils contained sufficient Fe(II) to catalyse some jarosite transformation (Grigg et al., 2024a; Jones et al., 2009; Karimian et al., 2017, 2018) and the pH was sufficiently high to allow Fe(II)-catalysed jarosite transformation in some pure mineral mesh bags (Karimian et al., 2017, 2018). Furthermore, native Fe oxyhydroxides in the soil could have been expected to accelerate the formation of Fe oxyhydroxides by providing a template for mineral growth from aqueous Fe(II) (Liu et al., 2022; Notini et al., 2022). Iron oxyhydroxides were minor phases in incubated soil for several reasons. Firstly, Fe(II) was stabilised by the soil matrix as adsorbed species or ferrous or mixed-valent minerals and was fit as phase D2a (Table 1). Secondly, the reduction of natural-isotope-abundance Fe in native soil minerals, which is dominated by ^{56}Fe, could have contributed to a dilution of ^{57}Fe in product phases formed inside the mesh bags by the Fe(II)-catalysed pathway (Notini et al., 2023).

In addition to the stabilisation of Fe(II) in the mesh bags, loss of ^{57}Fe, and possible inflow of ^{NA}Fe from the soil, are evidenced by the decreasing fraction of ^{57}Fe measured in the digestions of soils from the mesh bags. The loss of ^{57}Fe from the mesh bags could have resulted in the increased dominance of the initial phases in soil in the Mössbauer signal if those native phases were more resistant to reduction than the synthetic jarosite enrichment. Furthermore, the oxidation of ^{57}Fe(II) on the surface of clays (Géhin et al., 2007), or exchange between ^{57}Fe from dissolved jarosite and Fe in clays (Neumann et al., 2015) could have contributed to an increased ^{57}Fe signal of phases contained in the initial soil. Indeed, this interpretation is supported by the increase in the area of phase D3 during the incubation (Figs. 3 and 4). This phase has parameters similar to those measured in the initial soil attributed to Fe(III) in clays or organic complexes (Chen and Thompson, 2021; Lee et al., 2012; Notini et al., 2023; Winkler et al., 2018). Additionally, phase S2, which also appeared in the initial soil (Fig. 3A and Fig. 3K), increased in prominence during the incubation (compare Fig. 3B, 3E, 3H and 3L with Fig. 3C-D, F-G, I-J, and M-N, respectively; Fig. 4).

Unlike the Mössbauer spectra from pure mineral mesh bags, the Mössbauer spectra collected at 5 K from jarosite-enriched topsoil incubations contain prominent collapsed features. The features are similar to the transformation products of Fe oxyhydroxides in contact with a soil matrix (Notini et al., 2023; Schulz et al., 2023), but the phases cannot be clearly identified due to a lack of distinctive peaks and could include various Fe species. In general, collapsed features at 5 K are indicative of poorly crystalline or non-crystalline Fe compounds, either due to inhibited crystal growth, high degrees of substitution for Fe in crystals or organic complexation of Fe atoms (Chen and Thompson, 2021; Schulz et al., 2023; Thompson et al., 2011; Winkler et al., 2018). Some of the collapsed features follow the general form of a poorly-ordered octet, which could be a poorly crystalline green-rust-like mineral based on an octet fitting model (Notini et al., 2023), or Fe(II) sorbed to the surface of magnetically ordered Fe mineral phases (Winkler et al., 2018). Green rust is found in soils naturally (Feder et al., 2005), has formed following incubation of ferrihydrite-enriched soils (Notini et al., 2023), and is a known transformation product of jarosite (Karimian et al., 2017, 2018). High Fe(II) concentrations are required to form green rust, which may have been favoured in these samples due to slow diffusion of dissolved species in the clay soil. Although considered a metastable product of jarosite transformation (Karimian et al., 2017, 2018), green rust could be stabilised in anoxic soil media (Feder et al., 2005). Other ferrous or mixed-valence minerals that have low magnetic blocking temperatures may also contribute to the signal although siderite and vivianite are not likely to form in these soils. The fitting of collapsed features is discussed in Section S8.1.

Whereas there was a substantial difference in the products formed in pure-mineral and jarosite-enriched-soil mesh bags, corresponding large differences in the rates of jarosite transformation were not observed. Jarosite mixed with soil was transformed into secondary phases in 4–8 weeks in topsoil incubated in both mesocosms and field. In subsoil, the transformation was incomplete in sixteen weeks in mesocosms, and mostly transformed in the field. Considering that the contrasting products of transformation of jarosite in mesh bags containing pure mineral and mineral-enriched soil strongly indicated that the transformation of jarosite proceeded by different pathways, the similar transformation rates are more likely to be coincidental than indicative of fundamental similarities between the systems.

4.3. Aluminium substitution stabilises jarosite most strongly when in pure-mineral mesh bags

In pure-mineral mesh bags, clear differences were observed in the

rate of unsubstituted and Al-jarosite transformation, but Al had a smaller effect on the rate of transformation in ^{57}Fe-jarosite-enriched soil. More Al-substituted jarosite than unsubstituted jarosite was present in pure-mineral mesh bags after sixteen weeks, indicating that Al stabilised jarosite against transformation in topsoils and subsoil, in both mesocosm and field incubations. This is consistent with the effect of Al on the jarosite transformation rate that was observed in mixed suspension experiments, where the rate of Fe(II)-catalysed transformation of unsubstituted jarosite was more than 2.5 times greater than jarosite with 8 % Al-for-Fe substitution (Grigg et al., 2024a). However, once mixed with soil, the rate of unsubstituted and Al-substituted jarosite transformation was not clearly different from one another.

Although some lack of distinction between treatments may be partially explained by the larger scatter in the results from mineral-enriched soil samples, due to uncertainties in the fitting of Mössbauer parameters, the trends in pure-mineral mesh bags were clearly not replicated in the ^{57}Fe-jarosite-enriched soils. It is likely that the different effect of Al in the two incubation systems was due to the different transformation processes that dominated in each system. Iron(II)-catalysed transformation was likely a dominant process in the pure-mineral mesh bags, whereas reductive dissolution was more dominant in ^{57}Fe-jarosite-enriched soil. Just as Al has a larger effect on the rate of Fe(II)-catalysed transformation of jarosite than the rate of hydrolysis (Grigg et al., 2024a), the results of this study could indicate that Al also has a small effect on the rates of reductive dissolution of jarosite.

Aluminium substitution of jarosite may also alter the products of jarosite transformation (Grigg et al., 2024a). In XRD patterns of the contents of pure-mineral mesh bags (Fig. 2), the amount of ferrihydrite and goethite does not differ strongly between incubations of unsubstituted and Al-substituted jarosite. However, the minor products in pure mineral mesh bags show a strong difference between Al treatments, demonstrating that Al can stabilise or promote the growth of poorly crystalline minerals. Effects of Al on the products of transformation was not observed in mineral-soil mixed incubations, which could be due to the presence of other ions in solution that could have diminished the scale of any effect of Al on the product composition.

4.4. Laboratory mesocosm and field incubations produced comparable results

Comparing the rate and products of transformation, the same general trends were observed in the laboratory mesocosm and field incubations. Jarosite transformation occurred at comparable rates and produced the same dominant transformation products. Somewhat higher variability between the mineralogy of triplicate samples from field incubations compared to the laboratory mesocosm experiments was not sufficient to alter the interpretation of the transformation experiment. Many differences in the minor products of transformation may be explained by variability between the replicates.

The similarities between the results of the laboratory mesocosm and field experiments under the conditions tested in this study suggest that the design of the laboratory study was able to mimic the dominant processes that influence jarosite transformation in an acid sulfate rice paddy field from the Bangkok plain. Importantly, the exchange of porewater between the incubated soil and mesh bags was a similar process in the laboratory mesocosms and the field. This kind of exchange is not possible in small microcosm experiments, where a build-up of Fe(II) during the reductive dissolution of the Fe mineral enrichment can promote the formation of green-rust-like minerals (Notini et al., 2023). On the other hand, the clayey soil texture may have limited diffusion and slowed Fe(II) loss from the mesh bag in comparison to the amount of Fe(II) loss observed from the transformation of ferrihydrite and lepidocrocite in sandy soils (Schulz et al., 2023).

The most significant difference between the laboratory mesocosm and field incubations was the rate of jarosite transformation in the subsoil. Whereas almost no jarosite transformation occurred in the mesocosm subsoil within sixteen weeks, substantial transformation of jarosite occurred in the subsoils in the field. The faster transformation of jarosite during the field incubation may have been due to the higher pH in the field incubation (pH 6.2 – 6.5) than in the laboratory incubation (pH 3.6 – 3.7). Furthermore, the increased rate of jarosite transformation at 70 cm in the field, the formation of Fe(II) phases in Mössbauer spectra of ^{57}Fe-jarosite-enriched subsoils in the field, and the similarity in the amount of Fe lost from mesh bags in topsoil and subsoil due to reductive dissolution, suggest that Fe(II) reduction was sufficient at 70 cm depth in the field to influence the jarosite transformation processes. Indeed, measurements of the Fe concentration in porewater showed that porewater from the field contained more Fe than porewater from the mesocosms during the first eight weeks although the increasing Fe in the porewater at the end of the laboratory incubations was not associated with the formation of Fe(II) phases in Mössbauer spectra.

Visual inspection of the subsoils used for the field and lab experiment indicated that the experiments were conducted in similar horizons. Therefore, the differences may be caused by the treatment of the soil prior to the incubation. Mesocosm soils were dried, homogenised and reflooded, whereas the field soils retained their original structure and redox state at the beginning of the experiment. The established Eh values in the field were low enough to fall partially within the range of reduction of Fe from some compounds (Fig. S5; Fiedler et al., 2007; Reddy et al., 1986). By contrast, reducing conditions in the mesocosms established slowly. This may have contributed to the higher Eh of the subsoil mesocosms than the Eh of field subsoils, which had average Eh values of +466 mV and +275 mV throughout the sixteen-week experiment, respectively. A small difference between the microbial Fe reduction capacity of the field and mesocosm soils could have caused substantial difference in the rate and products of the jarosite transformation.

4.5. Implications

The stability of jarosite in soil is strongly influenced by the porewater geochemistry, solid matrix composition and jarosite mineral characteristics. Both mesocosms and field experiments showed that the products of the jarosite transformation are strongly influenced by the balance between competing transformation processes – reductive dissolution, dissolution by hydrolysis and Fe(II)-catalysed transformation processes – which are influenced by the properties of the reaction media and the minerals themselves. In pure-mineral mesh bags, the dominance of goethite among the transformation products is consistent with the Fe(II)-catalysed transformation of jarosite (Grigg et al., 2024a). By contrast, in the ^{57}Fe-jarosite-enriched soil mesh bags, reductive dissolution was the dominant pathway of jarosite transformation, and poorly crystalline or non-crystalline products were formed. This result demonstrates the potential importance of Fe(II) in organic complexes, Fe(II) sorbed to mineral surfaces, or Fe(II) bound within SRO or poorly crystalline minerals as products of jarosite transformation in soil. The prominence of non-mineral, SRO or poorly crystalline Fe(II) minerals, and the suppression or delay of crystalline Fe oxyhydroxide formation following jarosite transformation, could have consequences for the mobility and availability of major and trace elements, including nutrients and pollutants that were previously bound to the jarosite phase and have an affinity to Fe oxyhydroxides in soil.

In terms of transformation rate, the incubation of jarosite in both the laboratory mesocosms and the field demonstrated that jarosite transformation in paddy soil is up to three orders of magnitude slower than previously observed in mixed suspension systems (Grigg et al., 2024a). Therefore, jarosite may be stable in soils for longer than implied by mixed suspension experiments that have been carried out previously. Moreover, Al had a stronger effect on the transformation rate in samples where Fe(II)-catalysed transformation dominated over reductive dissolution of jarosite, demonstrating the importance of the balance between the competing transformation pathways in different soil environments

to understand the stability of jarosite in natural systems. Nonetheless, synthetic jarosite minerals were substantially or entirely reacted within the span of a single rice growing season (typically 3–5 months) when Fe reducing conditions prevailed in the soil. Therefore, the environmental effects of the jarosite transformation reactions are highly relevant on the timescales of the redox fluctuation observed in rice paddy fields.

5. Conclusions

Jarosite is an abundant mineral in ASS, and the soil-based incubation used in this study provides new information that explains the stability of jarosite in ASS. The results demonstrate how the contrasting geochemical conditions in topsoil and subsoil lead to different transformation rates and products of jarosite. Furthermore, the experiments show that the rate and products of transformation are a result of differing pathways of transformation that are dependent on the geochemical environment of the jarosite undergoing transformation. While the structure of the mineral itself, such as the degree of substitution of the jarosite by Al, may affect the rate and products of the transformation, this is highly dependent on the dominant transformation pathways. The results of this study provide new understanding of the processes that influence the stability of jarosite in oxidised ASS during cultivation, aging, or rehabilitation of the soil, and demonstrates the potential importance of studying the specifics of jarosite transformations in ASS environments.

CRediT authorship contribution statement

Andrew R.C. Grigg: Writing – original draft, Visualization, Methodology, Investigation, Formal analysis, Conceptualization. **Worachart Wisawapipat:** Writing – review & editing, Methodology, Investigation. **Kurt Barmettler:** Methodology, Investigation. **Katrin Schulz:** Writing – review & editing, Methodology. **Luiza Notini:** Writing – review & editing, Methodology. **Laurel K. ThomasArrigo:** Writing – review & editing, Supervision, Methodology, Conceptualization. **Ruben Kretzschmar:** Writing – review & editing, Supervision, Project administration, Methodology, Funding acquisition, Conceptualization.

Data availability

Data are available through ETH Zurich Research Collection at https://doi.org/10.3929/ethz-b-000666563.

Declaration of competing interest

The authors declare that they have no known competing financial interests or personal relationships that could have appeared to influence the work reported in this paper.

Acknowledgements

We gratefully acknowledge Noppadol Prayoonsuk and Nalinphorn Yimnoi (Chanchoengsao Rice Research Centre) for access to the field site, and sincerely thank Juthamard Kaiphoem, Parapond Leksungnoen, Arnon Nansahwang and Jirapat Tuntrachanida (Kasetsart University) for assistance in the field. Fieldwork was approved by the National Research Council Thailand (NRCT) (permit: 0002/1164) and the importation of soil samples to Switzerland was approved by the Federal Office of Agriculture (FOAG) under permit No. 17/21. This research is part of a project that has received funding from the European Research Council (ERC) under the European Union's Horizon 2020 research and innovation program (788009-IRMIDYN-ERC-2017-ADG).

Appendix A. Supplementary material

The supplementary material contains additional results and explanations on the topics: (S1) site description, (S2) mineral synthesis, (S3) sample holder design, (S4) experimental lay-out, (S5) porewater characterisation, (S6) isotope abundance analysis, (S7) X-ray diffraction, and (S8) Mössbauer spectroscopy. Supplementary material to this article can be found online at https://doi.org/10.1016/j.gca.2024.07.026.

References

Alpers, C.N., Nordstrom, D.K., Ball, J.W., 1989. Solubility of jarosite solid solutions precipitated from acid mine waters, Iron Mountain, California, U.S.A. Sci. Géol., Bull. Mémoires 42, 281–298.

Boland, D.D., Collins, R.N., Glover, C.J., Waite, T.D., 2013. An *in situ* quick-EXAFS and redox potential study of the Fe(II)-catalysed transformation of ferrihydrite. Colloids Surf. A Physicochem. Eng. Asp. 435, 2–8.

Boland, D.D., Collins, R.N., Miller, C.J., Glover, C.J., Waite, T.D., 2014. Effect of solution and solid-phase conditions on the Fe(II) accelerated transformation of ferrihydrite to lepidocrocite and goethite. Environ. Sci. Tech. 48, 5477–5485.

Bridge, T.A.M., Johnson, D.B., 2000. Reductive dissolution of ferric iron minerals by *Acidiphilium* SJH. Geomicrobiol J. 17, 193–206.

Byrne, J., Kappler, A., 2019. Mössbauer Spectroscopy, in: Kenney, J., Veeramani, H., Alessi, D. (Eds.), Analytical geomicrobiology: A handbook of instrumental techniques. Cambridge University Press, Cambridge, pp. 314-338.

Byrne, J., Kappler, A., 2022. A revised analysis of ferrihydrite at liquid helium temperature using Mössbauer spectroscopy. Am. Miner. 107, 1643–1651.

Cahyani, V.R., Murase, J., Ikeda, A., Taki, K., Asakawa, S., Kimura, M., 2008. Bacterial communities in iron mottles in the plow pan layer in a Japanese rice field: estimation using PCR-DGGE and sequencing analyses. Soil Sci. Plant Nutr. 54, 711–717.

Chen, C., Thompson, A., 2018. Ferrous iron oxidation under varying pO_2 levels: the effect of Fe(II)/Al(III) oxide minerals and organic matter. Environ. Sci. Tech. 51, 597–606.

Chen, C., Kukkadapu, R., Lazareva, O., Sparks, D.L., 2017. Solid-phase Fe speciation along the vertical redox gradients in floodplains using XAS and Mössbauer spectroscopies. Environ. Sci. Tech. 51, 7903–7912.

Chen, C., Thompson, A., 2021. The influence of native soil organic matter and minerals on ferrous iron oxidation. Geochim. Cosmochim. Acta 292, 254–270.

Cuttler, A.H., Man, V., Cranshaw, T.E., Longworth, G., 1990. A Mössbauer study of green rust precipitates: I. Preparations from Sulphate Solutions. Clay Miner. 25, 289–301.

Dutrizac, J.E., Jambor, J.L., 2000. Jarosites and their application in hydrometallurgy. Rev. Mineral. Geochem. 40, 405–452.

Elwood Madden, M.E., Madden, A.S., Rimstidt, J.D., Zahrai, S., Kendall, M.R., Miller, M. A., 2012. Jarosite dissolution rates and nanoscale mineralogy. Geochim. Cosmochim. Acta 91, 306–321.

Feder, F., Trolard, F., Klingelhöfer, G., Bourrié, G., 2005. In situ Mössbauer spectroscopy: evidence for green rust (fougerite) in a gleysol and its mineralogical transformations with time and depth. Geochim. Cosmochim. Acta 69, 4463–4483.

Fiedler, S., Vepraskas, M.J., Richardson, J.L., 2007. Soil redox potential: Importance, field measurement, and observations. Adv. Agron. 94, 1–54.

Gao, K., Jiang, M., Guo, C., Zeng, Y., Fan, C., Zhang, J., Reinfelder, J.R., Huang, W., Lu, G., Dang, Z., 2019. Reductive dissolution of jarosite by a sulfate reducing bacterial community: secondary mineralization and microflora development. Sci. Total Environ. 690, 1100–1109.

Géhin, A., Grenèche, J.M., Tournassat, C., Brendlé, J., Rancourt, D.G., Charlet, L., 2007. Reversible surface-sorption-induced electron-transfer oxidation of Fe(II) at reactive sites on a synthetic clay mineral. Geochim. Cosmochim. Acta 71, 863–867.

Goodman, B.A., Cheshire, M.V., Chadwick, J., 1991. Characterization of the Fe(III)-fulvic acid reaction by Mössbauer spectroscopy. J. Soil Sci. 42, 25–38.

Grigg, A.R.C., ThomasArrigo, L.K., Schulz, K., Rothwell, K.A., Kaegi, R., Kretzschmar, R., 2022. Ferrihydrite transformations in flooded paddy soils: rates, pathways, and product spatial distributions. Environ. Sci: Process. Impacts 24, 1867–1882.

Grigg, A.R.C., Notini, L., Kaegi, R., ThomasArrigo, L.K., Kretzschmar, R., 2024a. Aluminium substitution affects jarosite transformation to iron oxyhydroxides in the presence of aqueous Fe(II). Geochim. Cosmochim. Acta 374, 72–84.

Grigg, A.R.C., Notini, L., Kaegi, R., ThomasArrigo, L.K., Kretzschmar, R., 2024b. Structural effects of aluminum and iron occupancy in minerals of the jarosite-alunite solid solution. ACS Earth Space Chem. 8, 194–206.

Hansel, C.M., Benner, S.G., Fendorf, S., 2005. Competing Fe(II)-induced mineralization pathways of ferrihydrite. Environ. Sci. Tech. 39, 7147–7153.

IUSS Working Group WRB 2015. World Reference Base for Soil Resources 2014, update 2015. International soil classification system for naming soils and creating legends for soil maps., World Soil Resources Reports No. 106. FAO, Rome.

IUSS Working Group WRB 2022. World Reference Base for Soil Resources. International soil classification system for naming soils and creating legends for soil maps. 4th edition. International Union of Soil Sciences (IUSS), Vienna, Austria.

Ivarson, K.C., Hallberg, R.O., 1976. Formation of mackinawite by the microbial reduction of jarosite and its application to tidal sediments. Geoderma 16, 1–7.

Johnston, S.G., Burton, E.D., Keene, A.F., Planer-Friedrich, B., Voegelin, A., Blackford, M. G., Lumpkin, G.R., 2012. Arsenic mobilization and iron transformations during sulfidization of As(V)-bearing jarosite. Chem. Geol. 334, 9–24.

Jones, A.M., Collins, R.N., Rose, J., Waite, T.D., 2009. The effect of silica and natural organic matter on the Fe(II)-catalysed transformation and reactivity of Fe(III) minerals. Geochim. Cosmochim. Acta 73, 4409–4422.

Jones, E.J.P., Nadeau, T.-L., Voytek, M.A., Landa, E.R., 2006. Role of microbial iron reduction in the dissolution of iron hydroxysulfate minerals. J. Geophys. Res. 111, G01012.

Karimian, N., Johnston, S.G., Burton, E.D., 2017. Antimony and arsenic behaviour during Fe(II)-induced transformation of jarosite. Environ. Sci. Tech. 51, 4259–4268.

Karimian, N., Johnston, S.G., Burton, E.D., 2018. Antimony and arsenic partitioning during Fe^{2+}-induced transformation of jarosite under acidic conditions. Chemosphere 195, 515–523.
Karimian, N., Johnston, S.G., Tavakkoli, E., Frierdich, A.J., Burton, E.D., 2023. Mechanisms of arsenic and antimony co-sorption onto jarosite: An x-ray absorption spectroscopic study. Environ. Sci. Tech. 57, 4813–4820.
Karna, R.R., Noerpel, M.R., Nelson, C., Elek, B., Herbin-Davis, K., Diamond, G., Bradham, K., Thomas, D.J., Scheckel, K.G., 2021. Bioavailable soil Pb minimized by in situ transformation to plumbojarosite. PNAS 118.
Keene, A.F., Johnston, S.G., Bush, R.T., Sullivan, L.A. and Burton, E.D. 2010. Reductive dissolution of natural jarosite in a tidally inundated acid sulfate soil: Geochemical implications, 19th World Congress of Soil Science, Soil Solutions for a Changing World, Brisbane, Australia.
Kölbl, A., Kaiser, K., Winkler, P., Mosley, L., Fitzpatrick, R., Marschner, P., Wagner, F.E., Häusler, W., Mikutta, R., 2021. Transformation of jarosite during simulated remediation of a sandy sulfuric soil. Sci. Total Environ. 773, 145546.
Kölbl, A., Kaiser, K., Thompson, A., Mosley, L.M., Fitzpatrick, R.W., Marschner, P., Sauheitl, L., Mikutta, R., 2022. Rapid remediation of sandy sulfuric subsoils using straw-derived dissolved organic matter. Geoderma 420, 115875.
Kraal, P., van Genuchten, C.M., Lenstra, W.K., Behrends, T., 2020. Coprecipitation of phosphate and silicate affects environmental iron (oxyhydr)oxide transformations: A gel-based diffusive sampler approach. Environ. Sci. Tech. 54, 12795–12802.
Lacroix, E.M., Aeppli, M., Boye, K., Brodie, E., Fendorf, S., Keiluweit, M., Naughton, H.R., Noël, V., Sihi, D., 2023. Consider the anoxic microsite: Acknowledging and appreciating spatiotemporal redox heterogeneity in soils and sediments. ACS Earth Space Chem. 7, 1592–1609.
Land Development Department 2004. Characterization of established soil series in the central plain region of Thailand reclassified according to soil taxonomy 2003. Land Development Department (Thailand), Bangkok.
Lee, J.-H., Fredrickson, J.K., Kukkadapu, R.K., Boyanov, M.I., Kemner, K.M., Lin, X., Kennedy, D.W., Bjornstad, B.N., Konopka, A.E., Moore, D.A., Resch, C.T., Phillips, J. L., 2012. Microbial reductive transformation of phyllosilicate Fe(III) and U(VI) in fluvial subsurface sediments. Environ. Sci. Tech. 46, 3721–3730.
Liu, J., Sheng, A., Li, X., Arai, Y., Ding, Y., Nie, M., Yan, M., Rosso, K.M., 2022. Understanding the importance of labile Fe(III) during Fe(II)-catalyzed transformation of metastable iron oxyhydroxides. Environ. Sci. Tech. 56, 3801–3811.
Menchetti, S., Sabelli, C., 1976. Crystal chemistry of the alunite series: crystal structure refinement of alunite and synthetic jarosite. Neues Jahrb. Für Mineral. Monatshefte 406–417.
Murad, E., Schwertmann, U., 1983. The influence of aluminium substitution and crystallinity on the Mössbauer spectra of goethite. Clay Miner. 18, 301–312.
Neumann, A., Wu, L., Li, W., Beard, B.L., Johnson, C.M., Rosso, K.M., Frierdich, A.J., Scherer, M.M., 2015. Atom exchange between aqueous Fe(II) and structural Fe in clay minerals. Environ. Sci. Tech. 49, 2786–2795.
Nielsen, S.S., Kjeldsen, P., Hansen, H.C.B., Jakobsen, R., 2014. Transformation of natural ferrihydrite aged *in situ* in As, Cr and Cu contaminated soil studied by reaction kinetics. J. Appl. Geochem. 51, 293–302.
Notini, L., ThomasArrigo, L.K., Kaegi, R., Kretzschmar, R., 2022. Coexisting goethite promotes Fe(II)-catalyzed transformation of ferrihydrite to goethite. Environ. Sci. Tech. 56, 12723–12733.
Notini, L., Schulz, K., Kubeneck, L.J., Grigg, A.R.C., Rothwell, K.A., Fantappiè, G., ThomasArrigo, L.K., Kretzschmar, R., 2023. A new approach for investigating iron mineral transformations in soils and sediments using ^{57}Fe-labelled minerals and ^{57}Fe Mössbauer spectroscopy. Environ. Sci. Tech. 57, 10008–10018.
Ouyang, B., Lu, X., Liu, H., Li, J., Zhu, T., Zhu, X., Lu, J., Wang, R., 2014. Reduction of jarosite by Shewanella oneidensis MR-1 and secondary mineralization. Geochim. Cosmochim. Acta 124, 54–71.
Pedersen, H.D., Postma, D., Jakobsen, R., Larsen, O., 2005. Fast transformation of iron oxyhydroxides by the catalytic action of aqueous Fe(II). Geochim. Cosmochim. Acta 69, 3967–3977.
Poch, R.M., Thomas, B.P., Fitzpatrick, R.W., Merry, R.H., 2009. Micromorphological evidence for mineral weathering pathways in a coastal acid sulfate soil sequence with Mediterranean-type climate, South Australia. Aust. J. Soil Res. 47, 403–422.
Reddy, K.R., Feijtel, T.C., Patrick, W.H., 1986. Effect of soil redox conditions on microbial oxidation of organic matter. In: Chen, Y., Avnimelech, Y. (Eds.), The Role of Organic Matter in Modern Agriculture. Springer, Netherlands, Dordrecht, pp. 117–156.
Ruecker, A., Schröder, C., Byrne, J., Weigold, P., Behrens, S., Kappler, A., 2016. Geochemistry and mineralogy of Western Australian salt lake sediments: implications for Meridiani Planum on Mars. Astrobiology 16, 525–538.
Ryu, J.-G., Kim, Y., 2022. Mineral transformation and dissolution of jarosite coprecipitated with hazardous oxyanions and their mobility changes. J. Hazard. Mater. 427, 128283.
Scarlett, N.V.Y., Madsen, I.C., 2006. Quantification of phases with partial or no known crystal structures. Powder Diffr. 21, 278–284.
Schröder, C., Wan, M., Butler, I.B., Tait, A., Peiffer, S., McCammon, C.A., 2020. Identification of mackinawite and constraints on its electronic configuration using Mössbauer Spectroscopy. Minerals 10, 1090.
Schulz, K., Notini, L., Grigg, A.R.C., Kubeneck, L.J., Wisawapipat, W., ThomasArrigo, L. K., Kretzschmar, R., 2023. Contact with soil impacts ferrihydrite and lepidocrocite transformations during redox cycling in a paddy soil. Environ. Sci.: Process Impacts 53, 1945–1961.
Soil Survey Staff, 2015. Illustrated guide to soil taxonomy, version 2. U.S. Department of Agriculture, Natural Resources Conservation Service, National Soil Survey Center, Lincoln, Nebraska.
Stoffregen, R.E., Alpers, C.N., Jambor, J.L., 2000. Alunite-jarosite crystallography, thermodynamics and geochronology. Rev. Mineral. Geochem. 40, 454–479.
Sukitprapanon, T., Suddhiprakarn, A., Kheoruenromne, I., Anusontpornperm, S., Gilkes, R.J., 2016. A comparison of potenital, active and post-active acid sulfate soils in Thailand. Geoderma Reg. 7, 346–356.
Sukitprapanon, T., Suddhiprakarn, A., Kheoruenromne, I., Anusontpornperm, S., Gilkes, R.J., 2020. Nature of redox concentrations in a sequence of agriculturally developed acid sulfate soils in Thailand. Pedosphere 30, 390–404.
Taylor, P.D.P., Maeck, R., De Bièvre, P., 1992. Determination of the absolute isotopic composition and Atomic Weight of a reference sample of natural iron. Int. J. Mass Spectrom. 121, 111–125.
Thiel, J., Byrne, J.M., Kappler, A., Schink, B., Pester, M., 2019. Pyrite formation from FeS and H_2S is mediated through microbial redox activity. PNAS 116, 6897–6902.
ThomasArrigo, L.K., Mikutta, C., Byrne, J., Kappler, A., Kretzschmar, R., 2017. Iron(II)-catalyzed iron atom exchange and mineralogical changes in iron-rich organic freshwater flocs: An iron isotope tracer study. Environ. Sci. Tech. 51, 6897–6907.
ThomasArrigo, L.K., Byrne, J., Kappler, A., Kretzschmar, R., 2018. Impact of organic matter on iron(II)-catalyzed mineral transformations in ferrihydrite-organic matter coprecipitates. Environ. Sci. Tech. 52, 12316–12326.
Thompson, A., Rancourt, D.G., Chadwick, O.A., Chorover, J., 2011. Iron solid-phase differentiation along a redox gradient in basaltic soils. Geochim. Cosmochim. Acta 75, 119–133.
Tronc, E., Belleville, P., Jolivet, J.-P., 1992. Transformation of ferric hydroxide into spinel by Fe^{II} adsorption. Langmuir 8, 313–319.
Trueman, A.M., McLaughlin, M.J., Mosley, L.M., Fitzpatrick, R.W., 2020. Composition and dissolution kinetics of jarosite-rich segregations extracted from an acid sulfate soil with sulfuric material. Chem. Geol. 543, 119606.
Van Breemen, N., 1982. Genesis, morphology and classification of acid sulfate soils in coastal plains. In: Kittrick, J.A., Fanning, D.S., Hossner, L.R. (Eds.), Acid Sulfate Weathering. Soil Science Society of America, Madison, WI, USA, pp. 37–56.
Van Breemen, N., Harmsen, K., 1975. Translocation of iron in acid sulfate soils: I. Soil morphology, and the chemistry and mineralogy of iron in a chronosequence of acid sulfate soils. Soil Sci. Soc. Am. J. 39, 1140.
Vithana, C.L., Sullivan, L.A., Bush, R.T., Burton, E.D., 2013. Acidity fractions in acid sulfate soils and sediments: contributions of schwertmannite and jarosite. Soil Res. 51, 203–214.
Vithana, C.L., Sullivan, L.A., Burton, E.D., Bush, R.T., 2015. Stability of schwertmannite and jarosite in an acidic landscape: prolonged field incubation. Geoderma 239–240, 47–57.
Vogelsang, V., Fiedler, S., Jahn, R., Kaiser, K., 2016. *In-situ* transformation of iron-bearing minerals in marshland-derived paddy subsoil. Eur. J. Soil Sci. 67, 676–685.
Wan, M., Schröder, C., Peiffer, S., 2017. Fe(III):S(-II) concentration ratio controls the pathway and the kinetics of pyrite formation during sulfidation of ferric hydroxides. Geochim. Cosmochim. Acta 217, 334–348.
Welch, S.A., Christy, A.G., Kirste, D., Beavis, S.G., Beavis, F.R., 2007. Jarosite dissolution I - Trace cation flux in acid sulfate soils. Chem. Geol. 245, 183–197.
Winkler, P., Kaiser, K., Thompson, A., Kalbitz, K., Fiedler, S., Jahn, R., 2018. Contrasting evolution of iron phase composition in soils exposed to redox fluctuations. Geochim. Cosmochim. Acta 235, 89–102.
Yang, L., Steefel, C.I., Marcus, M.A., Bargar, J.R., 2010. Kinetics of Fe(II)-catalyzed transformation of 6-line ferrihydrite under anaerobic flow conditions. Environ. Sci. Tech. 44, 5469–5475.
Yee, N., Shaw, S., Benning, L.G., Nguyen, T.H., 2006. The rate of ferrihydrite transformation to goethite via the Fe(II) pathway. Am. Mineral. 91, 92–96.